HHS Public Access

Author manuscript

Nat Neurosci. Author manuscript; available in PMC 2022 April 25.

Published in final edited form as:

Nat Neurosci. 2021 November ; 24(11): 1555–1566. doi:10.1038/s41593-021-00929-y.

Context-Dependent Representations of Movement in *Drosophila* Dopaminergic Reinforcement Pathways

Aryeh Zolin[1], **Raphael Cohn**[1,*], **Rich Pang**[2,*], **Andrew F. Siliciano**[1,*], **Adrienne L. Fairhall**[2], **Vanessa Ruta**[1,3]

[1]Laboratory of Neurophysiology and Behavior, The Rockefeller University, New York, NY

[2]Neuroscience Graduate Program, Department of Physiology and Biophysics and Computational Neuroscience Center, University of Washington, Seattle, WA 98195 USA

Abstract

Dopamine plays a central role in motivating and modifying behavior, serving to invigorate current behavioral performance and guide future actions through learning. Here we examine how this single neuromodulator can contribute to such diverse forms of behavioral modulation. By recording from the dopaminergic reinforcement pathways of the *Drosophila* mushroom body during active odor navigation, we reveal how their ongoing motor-associated activity relates to goal-directed behavior. We find that dopaminergic neurons correlate with different behavioral variables depending on the specific navigational strategy of an animal, such that the activity of these neurons preferentially reflects the actions most relevant to odor pursuit. Furthermore, we show that these motor correlates are translated to ongoing dopamine release and acutely perturbing dopaminergic signaling alters the strength of odor tracking. Context-dependent representations of movement and reinforcement cues are thus multiplexed within the mushroom body dopaminergic pathways, enabling them to coordinately influence both ongoing and future behavior.

Introduction

Neuromodulators confer flexibility to neural circuits, endowing animals with the ability to adapt to a complex and ever-changing world[1]. Across invertebrates and vertebrates alike, the neuromodulator dopamine influences diverse facets of behavior over different timescales. Dopamine has canonically been studied for its role in representing reward and stimuli predictive of reward, providing a teaching signal that drives learning[2–4]. Yet,

[3]Correspondence: ruta@rockefeller.edu.
[*]These authors contributed equally to this work

Author Contributions

A.Z. performed DAN imaging and behavioral experiments with assistance from R.C.; R.C. designed and created the closed-loop system and wrote custom code for data analysis with A.Z.; R.P. performed analysis and modeling with A.F.; A.S. performed functional characterization of different DAN subsets and patterns of dopamine release. A.Z. and V.R. wrote the manuscript with input from all the authors.

Competing Interests Statement

The authors declare no competing interests.

Code availability

Code used for processing and modeling of the data is available at https://github.com/rkp8000/mushroom_mushroom

loss of dopaminergic signaling also leads to pronounced motor and motivational deficits, highlighting a central role in both coordinating and invigorating an animal's actions[5–9]. Dopamine therefore subserves multiple seemingly disparate functions—shaping ongoing behavioral performance and modifying future behavior through learning.

How can a single neuromodulator exert such a broad influence on behavior? The diverse roles of dopamine could arise from functionally specialized and anatomically segregated circuits that each encode either reinforcement, motor, or motivational signals[6,10]. Alternatively, the same dopaminergic pathways could contribute to multiple forms of behavioral modulation. Indeed, recent recordings reveal that midbrain dopaminergic neurons responsive to rewards also display motor-associated activity as animals perform a learned task[11,12]. However, whether ongoing motor correlates in dopaminergic neurons simply encode motor kinematics, convey a motivational signal to promote reward-seeking behavior, or reflect the expectation of reward remains enigmatic[13–15]. Moreover, whether the multiplexed activity of dopaminergic neurons indicate that the same pathways can both rapidly shape online behavioral performance and instruct learning is unclear.

Here we took advantage of the concise circuitry of the mushroom body, the associative olfactory center of *Drosophila*, to gain insight into the dual representation of reward and motor activity by dopaminergic pathways. The mushroom body is richly innervated by dopaminergic neurons (DANs) whose segregated axonal projections target discrete, non-overlapping compartments that tile the length of the mushroom body's output lobes[16]. DANs innervating different compartments convey the reinforcement signals that instruct learning, with distinct subsets activated in response to either reward or punishment[17–24]. Each compartment of the mushroom body lobe is also innervated by the dendrites of 1–3 mushroom body output neurons (MBONs). Local dopamine release within a compartment can therefore tune the strength of synaptic connections between the Kenyon cells that encode odor identity and the MBONs that bias behavior, enabling the same olfactory cue to drive either approach or avoidance depending on an animal's past experience[16,22,23,25–28]. Recent studies have also revealed that the activity of specific mushroom body DANs correlates the spontaneous motor actions of an animal[26,29–31]. The mushroom body therefore offers the opportunity to explore motor-related signaling in a simplified dopaminergic circuit with a defined role in reinforcement learning.

To gain insight into the nature of motor-associated activity in DANs, we devised methods to record from the mushroom body as animals actively pursued an appetitive odor plume in a virtual olfactory environment, allowing us to directly compare ongoing dopaminergic activity during spontaneous and purposive behavior and disambiguate whether their signaling relates to the sensory stimulus, motor kinematics, or represents a context-dependent cue related to the task. We find that the same DANs responsive to reinforcement cues that instruct learning provide a rich representation of the moment-by-moment actions of an animal. Dopaminergic correlates of behavior, however, are not invariant but depend on the navigational strategy used for odor tracking, such that DANs preferentially represented the behavioral variables most relevant for pursuit. Together, our results suggest that rewards and purposive actions are encoded through comparable patterns of dopaminergic neuron activity and dopamine release, highlighting how the same neuromodulatory pathways can

contribute to multiple forms of behavioral modulation over diverse timescales—conveying motivational signals to rapidly shape current behavior as well instructive signals to modify future behavior through learning.

Results

Mushroom body DAN activity correlates with locomotion

To explore how dopaminergic pathways in the *Drosophila* mushroom body coordinately represent reward and movement, we monitored their activity in head-fixed animals walking on an air-supported, freely-rotating ball (Fig. 1A, Extended Data Fig. 1A). We expressed a synaptically localized calcium indicator GCaMP (sytGCaMP6s) under the tyrosine hydroxylase and dopa-decarboxylase drivers (TH/DDC), allowing us to visualize calcium influx in DAN axon terminals innervating the different compartments that tile the mushroom body lobes (Fig. 1A,B). We focused on the population of DANs targeting the γ lobe (γ2-γ5), as these respond to positive and negative contextual cues to instruct short-term associations[20,24,26]. Starved animals walking in the dark, in the absence of any overt stimuli, alternated between spontaneous bouts of locomotion and quiescence and when presented with a droplet of 1M sucrose, immediately ceased walking and consumed the sugar, allowing us to compare the activity evoked by reward and locomotion within the same trials (Fig. 1C).

As previously described, ingestion of sucrose evoked bidirectional changes in the γ lobe dopaminergic population[26], activating the γ4 and γ5 DANs while suppressing the γ2 and γ3 DANs. Prior to and after sugar consumption, fluctuations in DAN activity were also observed that appeared to be temporally aligned to an animal's locomotion (Fig. 1C). The relative magnitude of these reward and motor-associated signals differed across DAN subsets, pointing to their functional specialization. While γ4 DANs were robustly activated by both sugar ingestion and locomotion, γ2 and γ3 DANs were activated only during walking and inhibited by reward (Fig. 1C and Extended Data Fig. 1B). In contrast, sugar-evoked responses in the γ5 compartment were far larger than any motor-associated fluctuations (Fig. 1C and Extended Data Fig. 1B). To characterize the locomotor-related activity of DANs, we therefore focused on the γ2, γ3, and γ4 subpopulations.

The dual representation of locomotion and reward within a compartment could arise either from heterogeneous classes of DANs that target the same compartment or from the multiplexed activity of individual neurons. Recent connectomic analyses indicate that the γ4 DANs can be divided into distinct subclasses based on their patterns of pre-synaptic connectivity[32], raising the possibility that they comprise a functionally diverse population. Using intersectional genetic drivers, we recorded from two morphologically distinct γ4 DAN subpopulations that could be distinguished by the axonal tract they follow to innervate the lobes (Extended Data Fig. 1D,E; MB312B, upper commissure; MB316B, lower commissure). While both subsets exhibited robust motor-associated activity, MB316B+ γ4 DANs also responded to sugar ingestion (Extended Data Fig. 1F–H). To further explore the multiplexed activity of the MB316B+ subpopulation, we used constrained nonnegative matrix factorization[33] to identify clusters of correlated pixels within the γ4 compartment, which presumably correspond to the individual axonal boutons of

different neurons. Individual pixel clusters displayed both movement- and reward-related signals, an observation further corroborated by imaging of single MB312B+ and MB316B+ soma (Extended Data Fig. 2). Distinct DAN subclasses innervating the γ4 compartment thus appear to be functionally specialized, with a population selectively tuned to ongoing movement and a subset conveying multiplexed signals about locomotion and reward.

To assess whether the motor-associated activity of DANs can drive dopamine release, we expressed the genetically encoded dopamine sensor dLight1.3b[34] in Kenyon cells, their primary targets in the mushroom body (Fig. 1B,D). During bouts of locomotion, we observed rapid fluctuations in dLight signaling along the length of Kenyon cell axons that adhered to the compartmental organization of the γ lobe (Fig. 1B, Extended Data Fig. 1C, Supplementary Video 1). Dual recordings of DANs expressing the red calcium sensor jRGECO[35] and dLight in Kenyon cells demonstrated that dopamine release was highly correlated with DAN activity in the γ4 compartment, with comparable signals evoked by locomotion and reward (Fig. 1E,F). Despite the heterogeneity of γ4 DAN subclasses, we were unable to identify any functional topography or compartmental subdomains in either the activity of the broader DAN population labeled by TH/DDC or dLight signaling. Indeed, multiple clustering algorithms defined each compartment as a relatively homogenous functional unit (Fig. 1B and Extended Data Fig. 1C). Examination of the *Drosophila* connectome reveals that different DAN subclasses have highly intermingled pre-synaptic terminals within the γ4 compartment[32] (Extended Data Fig. 1E), suggesting a potential basis the spatially homogenous patterns of dopamine release evoked by both locomotion and reward.

Differential encoding of behavior across compartments

While information about ongoing locomotion could be globally broadcast across the brain[30], we observed that the DANs innervating different compartments reflected distinct facets of motor activity that unfolded over different timescales. For example, γ3 DAN activity consistently tracked the onset and offset of each bout of locomotion, independent of the heterogeneous kinematics of spontaneous movement (Fig. 2A,B). In contrast, γ2 and γ4 DAN activity was highly variable even for bouts of walking that were indistinguishable by multiple behavioral metrics, both within and across individuals (Fig. 2A–C and Extended Data Fig. 3A–F, Supplementary Fig. 1). Conversely, although γ3 DAN activity faithfully reflected walking bouts enduring for tens of seconds, it only weakly tracked the rapid fluctuations in an animal's velocity during periods of continuous locomotion (Fig. 2A, Extended Data Fig. 4A). Rather, increases in forward velocity were associated with increased γ4 activity and decreased γ2 activity, while increases in angular velocity (turning) were associated with increased γ2 and γ3 activity and decreased γ4 activity (Extended Data Fig. 4A–C). However, as observed for movement initiation, these relationships were inconsistent even within the same individuals (Extended Data Fig. 4A). Linear filters describing the moment-to-moment relationship between DAN activity and forward or angular velocity on average accounted for only a fraction of the variance in DAN activity during locomotion, but their predictive power varied widely between flies (Fig. 2D–F, Extended Data Fig. 3G). Filters generated from multiple DANs accounted for significantly more of the variance than any single dopaminergic compartment (Extended Data Fig. 4G),

suggesting that the ensemble activity of heterogenous DANs carries more information about an animal's ongoing behavior than an individual compartment.

During bouts of ongoing locomotion, the activity of different DANs was highly correlated on a sub-second time scale (Extended Data Fig. 4D–F). Yet, these intercompartmental relationships fluctuated rapidly (Extended Data Fig. 4D,H). Interestingly, the coordinated activity of DANs during locomotion partially mirror the responses of DANs evoked by sugar rewards or aversive shock[26] (Extended Data Fig. 4A–F, 5D), highlighting how the rich interconnectivity between compartments[16,26,32] may generate similar network states in response to both external reinforcements and ongoing behavior.

Recording DAN activity during active odor pursuit

Motor correlates in mammalian dopaminergic pathways have been proposed to reflect an animal's anticipation of reward or represent the motivation or vigor of goal-directed behaviors[5,7,10,11,36–40]. The variable mapping between mushroom body DAN activity and apparently indistinguishable movements during spontaneous locomotion raised the possibility that these neuromodulatory pathways, likewise, do not simply encode the kinematics of locomotion, but may be shaped by an animal's behavioral context. To explore this possibility, we devised methods to record from DANs as flies were engaged in active pursuit of an appetitive odor plume.

A common navigational strategy employed by many insects, including *Drosophila*, is to reorient and increase their upwind velocity in response to an attractive olfactory cue, leading them to the odor source[41]. Indeed, flies freely walking in constant airflow displayed robust upwind tracking in response to a brief pulse of the food odor apple cider vinegar (ACV) (Supplementary Fig. 2A–E). To replicate odor-evoked tracking under the microscope, we used a closed-loop olfactory paradigm in which the heading of a tethered fly walking on an air-supported ball was yoked to the rotation of a tube carrying either a clean or odorized airstream, enabling an animal to control its orientation within an olfactory plume[28] (Fig. 3A, Supplementary Fig. 2G). Tethered flies could thus track an appetitive plume by reorienting and maintaining a steady upwind heading, resulting in a net upwind displacement towards the fictive odor source (Fig. 3B and Supplementary Fig. 2D).

On average, the population of γ4 DANs was activated by brief pulses of ACV (Fig. 3D, Supplementary Video 2), consistent with their sensitivity to appetitive cues[18,20,26,31] (Fig. 1C,D and Extended Data Fig. 1B). However, odor-evoked responses were highly variable even between sequential odor presentations ("trials") within an individual animal (Fig. 3B,D). This variation appeared related to the concurrent behavioral response to the odor: γ4 DAN responses were strongest during trials when animals vigorously reoriented to track upwind and weaker when animals failed to alter their heading and continued to walk crosswind (Fig. 3B,F). Consequently, trial-by-trial, average γ4 DAN activity was correlated with the net distance an animal tracked upwind towards the fictive odor source (Fig. 3F, Extended Data Fig 5A,C). γ2 DAN activity also depended on an animal's behavioral response but in the opposite manner. These relationships were not apparent in clean air (Extended Data Fig. 5A–C), nor did they depend on differences in the efficacy of odor stimulation, as the magnitude of Kenyon cell responses was independent of the position

of the odor tube (Extended Data Fig. 3H). Thus during active olfactory pursuit, mushroom body DANs neither solely represent the presence of an odor cue nor the kinematics of movement, but rather reflect the behavioral response to the stimulus.

In the closed-loop paradigm, flies tracked towards the fictive odor source predominantly by altering their heading to reorient in the upwind direction, rather than increasing their forward walking speed (Fig. 3C, Extended Data Fig. 5B,C). Interestingly, the moment-to-moment correlation between γ4 DAN activity and these behavioral variables was differentially strengthened as animals transitioned from walking in clean air to odor pursuit, with a notable change in the γ4 DAN-|heading| filter (Fig. 3E). Likewise, across trials, an animal's average heading but not its forward velocity was correlated with the γ4 DAN response and inversely correlated with the γ2 DAN response (Fig. 3F and Extended Data Fig. 5A,D). Motor variables thus appear to be distinctly encoded by DANs as animals actively track an odor plume.

Context-dependent representations of odor-tracking behavior

The emergence of novel behavioral correlates during olfactory pursuit suggests that DAN representations of movement may depend on behavioral context. To explore this possibility, we altered the experimental conditions to induce flies to rely on a distinct navigational strategy to track towards the fictive odor source. By increasing the speed of the airflow, we observed that animals walked upwind almost continuously for several meters, even in the absence of odor (Fig. 4A), consistent with evidence that high airflow triggers positive anemotaxis in many insect species[42]. During these extended bouts of anemotaxis, the moment-to-moment correlations between γ2 and γ4 DAN activity and a fly's heading were strengthened compared to when animals walked in more circuitous paths in clean air under low airflow conditions (Extended Data Fig. 5G). Distinct behavioral correlates therefore arise as animals pursue a straight upwind trajectory, irrespective of whether tracking was elicited by high airflow or an appetitive odor.

Tethered flies walking upwind in high airflow responded to ACV by maintaining their current heading and transiently increasing their forward velocity (Fig. 4A,B, Extended Data Fig. 5F). As observed in the low airflow context, we found that as animals transitioned from walking in clean air to odor pursuit, the correlations between DAN activity and different behavioral variables changed, both in the structure of their moment-to-moment relationships captured by the linear filters (Fig. 4C) and in their averaged activity over the course of an odor trial (Fig. 4D). Notably, whereas in the low airflow context, the average γ4 DAN activity during the odor stimulus was predominantly correlated with changes in an animal's heading (Fig. 3F), in the high airflow context, it was more strongly correlated with an animal's forward velocity (Fig. 4D, Extended Data Fig. 5E, Supplementary Fig. 3A–D). These distinct relationships were apparent even if behavioral data was subsampled to have equivalent variance in low and high airflow regimes (Extended Data Fig. 5H,I). Despite the differential encoding of motor actions in low and high airflow, γ4 DAN activity remained well correlated with an animal's net upwind displacement in the odor plume across experimental conditions (Fig. 3F, 4D). Context-dependent correlations between DAN

activity and behavior thus emerge as flies engage in different odor tracking strategies, with the behavioral metrics most relevant to odor pursuit selectively strengthened in each.

A simple model for odor pursuit

We sought to understand how the rapid remapping of DAN activity to behavior, captured by the changing linear filters, might give rise to these longer timescale relationships that emerge during olfactory navigation. We found that simply applying the best-fit linear filter to the experimentally measured behavior (Fig. 5A) could largely reproduce the trial-by-trial relationships between DAN activity, an animal's specific motor actions and the net distance it tracked towards the odor source (Fig. 5B,C). For example, the filters fit to γ4 DAN activity as animals walked in odor in low airflow gave rise to a strong correlation between the average γ4 DAN activity and a fly's heading, but a weaker correlation with its forward velocity, replicating the experimentally-observed relationships (Fig. 5B). Conversely, the filters fit to γ4 DAN activity in high airflow predicted a strong correlation with the average forward velocity of an animal tracking the odor plume, but not its heading (Fig. 5C). These relationships did not depend on the behavioral kinematics of odor pursuit as applying the low airflow filters to the high airflow behavioral data replicated the DAN-behavior correlations displayed in the low airflow context (Fig. 5E and Extended Data Fig. 6B,D). Likewise, the high airflow filters were sufficient to reproduce the experimentally observed relationships when applied to the low airflow data (Fig. 5D and Extended Data Fig. 6A,C), reinforcing that these context-dependent correlations depend principally on the distinct structure of the linear filters across conditions. Moreover, these relationships were not present if we used filters fit to DAN activity when animals walked in clean air (Extended Data Fig. 6E,F). The context-dependent restructuring of ongoing DAN-motor correlates thus naturally give rise to the longer timescale relationships we observe, ultimately strengthening the representation of actions that subserve odor navigation.

To further illuminate how the relationships between DAN activity and behavior unfolded over an odor trial, we calculated a cross-correlation matrix at various temporal offsets relative to the odor stimulus. This analysis supports our observations that the moment-to-moment correlations between DAN activity and distinct behavioral variables were differentially strengthened as an animal entered the odor plume (Extended Data Fig. 7). Unexpectedly, the activity of some DANs became significantly correlated not only with an animal's current behavior, but also with its prospective tracking throughout the odor presentation (up to 8 sec into the future, Extended Data Fig. 7C,D). This anticipatory activity could not be explained by the possibility that animals maintain invariant trajectories within the odor plume, at least for the low airflow context, where the auto-correlation of their heading was predictive for < 3 sec and was similar in both clean air and odor (Extended Data Fig. 7B). A nested model quantifying how much the past, present, or future behavior contributed to predicting DAN activity further reinforced that DANs carry prospective signals (Extended Data Fig. 8A). In the low airflow context, while a fly's heading prior to odor onset had a negligible contribution to DAN activity, including current or future heading significantly improved the model's ability to predict γ4 activity in the initial epoch of an odor response (Extended Data Fig. 8B). In contrast, in the high airflow context, an animal's forward velocity, but not its heading, was the primary predictor of DAN activity in odor

(Extended Data Fig. 8C). The anticipatory signaling of the mushroom body DANs further underscores that these pathways are not simply reporting on an animal's instantaneous experience, but appear to reflect context-dependent computations spanning multi-second timescales.

Satiety state coordinately modulates DAN activity and behavior

Our functional evidence that DANs preferentially correlate with the actions relevant to odor pursuit suggests that they may, like mammalian reinforcement pathways, reflect goal-directed behavior. Given that hunger represents a critical and conserved regulator of motivational drive, we explored how satiety state coordinately alters DAN activity and odor pursuit by measuring both in the low airflow context prior to (starved) and after consumption of sucrose (fed). Once sated, tethered animals walked with lower velocity and more frequently failed to reorient and steer upwind in response to ACV (Fig. 6B and Supplementary Fig. 3E), mirroring the diminished odor attraction of fed freely moving flies (Supplementary Fig. 2F)[43,44]. The dampened behavioral attraction to ACV in fed flies was accompanied by a corresponding attenuation of DAN responses (Fig. 6C).

Nevertheless, on a trial-by-trial basis, γ4 DAN responses remained significantly correlated with the change in an animal's heading in the odor plume (Fig. 6A,D), indicating that this population was still activated on the trials when a fed fly did reorient to walk upwind towards the odor source. Indeed, filters fit to DAN activity in starved or fed animals comparably predicted the longer timescale DAN-movement relationships observed in either satiety state (Extended Data Fig. 9). Thus γ4 DANs remained preferentially correlated with contextually-relevant behavioral variables irrespective of an animal's hunger state. While metabolic signaling pathways are thought to directly impinge onto DANs[43,45], our results suggest that satiety state-dependent changes in DAN activity, at least in part, arise from the behavioral differences in starved and fed flies, underscoring the tight connection between internal state, locomotor activity, and motivational drive.

DAN activity influences ongoing behavior

The rapid context-dependent signaling of mushroom body dopaminergic pathways suggests that, beyond their established role in learning and memory, DANs may also acutely shape behavior. To test this possibility, we selectively expressed the light-gated anion channel, GtACR1, or cation channel, CsChrimson, in distinct subsets of DANs, allowing us to transiently inhibit or activate these populations during odor tracking in freely moving animals (Fig. 7A). To minimize the potential confounds of behavioral modulation due to learning, we examined odor pursuit in nominally naïve animals in response to a single brief episode of optogenetic illumination (Fig. 7B). The protocerebral anterior medial (PAM) DANs innervate multiple mushroom body compartments, including γ4, and their activation is sufficient to instruct appetitive odor associations[18,20,24,28]. Optogenetic inhibition of the entire cluster of PAM DANs, or just the MB312+ population of γ4 DANs, consistently suppressed attraction to ACV in starved flies (Fig. 7A–C and Extended Data Fig. 10A, Supplementary Fig. 4A). In contrast, silencing the protocerebral posterior lateral (PPL) DANs that convey negative reinforcement during learning[17,19,21,28] had no impact on odor tracking. Conversely, optogenetic activation of PAM DANs increased the proportion of fed

flies that tracked upwind towards an odor and even promoted upwind tracking in the absence of an odor stimulus (Fig. 7D and Extended Data Fig. 10B, Supplementary Fig. 4B,C). Acute manipulation of DANs therefore bidirectionally modulates olfactory approach behaviors, in accord with more chronic perturbations[44,46], with inhibition of PAM DANs suppressing the strong attraction of starved animals and their activation reversing the behavioral indifference of fed flies.

Discussion

In this study, we took advantage of the mushroom body's concise circuit architecture to explore the nature of movement-related activity in a population of dopaminergic neurons that instruct associative learning. While motor signals have been previously observed in the mushroom body DANs[26,29–31], by developing methods to examine their activity as an animal was actively engaged in odor tracking, we gain new insight into these motor correlates and how they contribute to adaptive behavior. Although DANs provide a rich representation of a fly's ongoing behavior, several lines of evidence suggest these motor correlates do not simply reflect the kinematics of movement. First, the relationship between DAN activity and indistinguishable motor actions is not fixed but can rapidly change to reflect alterations to an animal's context. Indeed, distinct DAN-motor correlations emerged as animals transitioned from walking in clean air to active odor pursuit, such that the representation of actions most relevant to odor tracking in a particular context were selectively strengthened (Fig. 8). As a consequence, $\gamma 4$ DAN activity consistently correlated with an animal's net upwind displacement towards the appetitive odor source on a given trial, irrespective of the specific navigational strategy used for tracking. Second, our analyses suggest how these moment-to-moment correlations give rise to longer timescale relationships, even extending beyond immediate behavior such that DANs carried information about an individual's prospective tracking within the odor plume. Finally, optogenetic perturbations of DAN activity acutely alters odor tracking, indicating that these pathways not only reflect but also modulate real-time behavior. Together, these data support a model in which DAN-motor correlates are dynamically tuned to the actions that subserve goal-directed and purposive behavior (Fig. 8), like seeking a food source, suggesting a fundamental connection between movement and motivation within these dopaminergic pathways.

Layered multiplexing of reward and motor signals

Our work supports emerging evidence that mushroom body DANs exhibit functional complexity beyond signaling rewards or punishments. DANs innervating different compartments reflect both external reinforcement cues[18,24,26] and motor variables, giving rise to a rich and distributed representation of an animal's ongoing experience through correlated patterns of activity across the population. The *Drosophila* connectome reveals how functional specialization within different DAN subsets may arise. Individual DANs display divergent patterns of synaptic connectivity[32], integrating from an array of interneurons emanating from additional higher-order neuropils, feedback from MBONs innervating different compartments, as well as select ascending sensory pathways. The mushroom body DANs are thus wired into a highly interconnected network, poised to

convey pre-processed signals that reflect an animal's external environment, internal state, motor actions, and motivations. The complexity of inputs to the DANs further suggests how their activity may be rapidly remapped to different behavioral actions depending on the context in which they are performed, either by inheriting context-dependent signals from their diverse presynaptic partners or reweighting these inputs in a context-dependent manner. Likewise, the highly recursive and integrative wiring of DANs suggests how both ingestion of a sucrose reward and tracking towards an appetitive odor source can generate comparable patterns of network activity.

Mirroring the multifaceted and complex functional representations, we find that the same DANs that instruct olfactory associations also acutely influence odor pursuit. These observations suggests that in *Drosophila* diverse forms of dopaminergic modulation may be subserved by the same neuronal pathways. Recent work suggests that mammalian striatal dopaminergic neurons display similar heterogenous and multiplexed activity in which representations of behavior and motivational cues are coupled with teaching signals[6,10–12], further supporting that functional diversity may be an important principle allowing dopaminergic systems to guide diverse forms of adaptive behavior.

Diverse computational roles for dopamine

An important remaining question is whether and how the targets of the mushroom body DANs—Kenyon cells and MBONs—differentiate between dopamine signals evoked by external reinforcements or arising from behavior. While subsets of γ4 DANs appear functionally specialized, their axonal projections are intermingled throughout the compartment and form similar numbers of synapses with the main γ lobe Kenyon cells[32]. This synaptic organization suggests that ongoing release of dopamine during locomotion may engage the same synaptic plasticity mechanisms that drive memory formation, allowing both rewards and self-generated actions to similarly modulate behavior. Although the goal of reinforcement learning is to shape an animal's long-term decision-making policies[47], short-term associations are required to solve the credit assignment problem and extract the causal relationship between an animal's actions and subsequent rewards. The combination of ongoing DAN activity during odor pursuit and rapid dopamine-dependent plasticity of the γ lobe offers a potential mechanism for storing such an eligibility trace of a fly's recent actions. For example, KC-to-MBON synapses activated by an odor during locomotion could be rendered sensitive to an ensuing reward, generating a short-term association useful for updating a fly's decision-making policy during odor navigation. Such a mechanism could underlie recent evidence for history-dependent odor tracking behavior[48] or facilitate pursuit of an odor plume. Indeed, optimization of a simulated mushroom body network for different tasks, including odor navigation, revealed highly distributed DAN activity patterns that covaried with multiple task-relevant variables, mirroring the multifaceted representations we experimentally observe[49].

Optimal behavioral policies may not only emerge through learning but could be hard wired into the nervous system through evolution to assure appropriate adaptive behavior. The mushroom body's position at the nexus of sensory circuits conveying odor signals and the efferent MBON pathways that bias behavior makes it an optimal substrate for dopaminergic

signaling to modulate olfactory behavior, whether based on an animal's past experience or its current context. Our data add to growing evidence that the mushroom body plays a role beyond associative learning[26,44,46], suggesting dopaminergic modulation may act through multiple mechanisms that function over distinct timescales. Consistent with this notion, the *Drosophila* connectome reveals that DANs synapse directly onto MBONs[32,50], providing a parallel route of communication that is mechanistically distinct from associative plasticity. Interestingly, the heterogenous subclasses of γ4 DANs differentially synapse onto the dendrites of three MBONs innervating the γ4 compartment[32], suggesting an additional mechanism to expand the computational capacity of a single compartment and to shape moment-to-moment behavior.

Conservation of neuromodulatory mechanisms

Our work supports the basic correspondence of dopaminergic systems in insects and mammals, despite their separation by several hundred million years of evolutionary divergence. Dopamine acts upon circuits that display a fundamentally different architecture across these distant phyla yet can give rise to similar forms of learning and adaptive behavior. Whether the analogous roles of dopamine in insects and mammals reflect the basic conservation of neuromodulatory pathways or convergent evolution is not clear[51]. One possibility is that dopamine's evolutionary ancient role as a modulator of motor circuits[52] predisposed dopaminergic systems to acquire more specialized functions as brain complexity evolved, linking reward pursuit and reinforcement. Alternatively, the ubiquity of dopamine as a modulator of associative circuits could reflect similar computations arising repeatedly, potentially taking advantage of conserved receptor signaling pathways and molecular hardware. In either case, the coupling of reinforcement signals and locomotor representations in the same neuromodulatory system across divergent taxa suggests an inherent connection between them. By representing and invigorating motor actions and assigning value to sensory stimuli through learning, dopaminergic pathways allow animals to flexibly adapt their behavior over different timescales: acutely shaping moment-by-moment movements to achieve short term goals and effecting persistent changes in behavior through learning.

Methods

Fly Husbandry

Flies were maintained on cornmeal-agar-molasses medium at 23–25°C, 60–70% relative humidity, under a 12-hour light/dark cycle and transferred to vials containing only a KimWipe soaked in 2 mL water (or 0.2 mM all-trans-retinal water for optogenetic experiments) 18–24 hours before all experiments. For optogenetic experiments, flies were grown on retinoid-free sugar-and-yeast-based food in complete darkness. 1–2-day-old-females were transferred to conventional food containing 0.4 mM all-trans-retinal (Sigma #R2500) and placed in the dark for ≥24 hours.

Fly Stocks and Genotypes

All experiments were performed using 1–7-day-old females. For detailed fly stock sources and genotypes see Supplementary Table 1.

Fly Tethering and Dissection

For *in vivo* imaging of neural activity, flies were prepared as described previously[53] with minor modifications. Briefly, 3–7-day-old-females were anesthetized using CO_2 (<30 sec) and tethered to a specially designed holder dish. The fly was held in place with UV-curable glue (Loctite) applied to each eye and thorax and the proboscis was glued in an extended position. Care was taken to avoid glue contacting the antennae or aristae. After a <2-hour recovery period, the dish was filled with external saline (108 mM NaCl, 5 mM KCl, 2 mM CaCl2, 8.2 mM MgCl2, 4 mM NaHCO3, 1 mM NaH2PO4, 5 mM trehalose, 10 mM sucrose, 5 mM HEPES sodium salt, pH 7.5 with osmolarity adjusted to 275 mOsm) and the cuticle covering the dorsal portion of the head was removed. Muscle 16 and obstructing trachea were removed with care taken to keep the antennae and antennal nerves intact.

Two-Photon Functional Imaging

All functional imaging experiments were performed on an Ultima two-photon laser scanning microscope (Bruker Nanosystems) equipped with galvanometers driving a Chameleon Ultra II Ti:Sapphire laser. Emitted fluorescence was detected with either photomultiplier-tube or GaAsP photodiode (Hamamatsu) detectors. Images were acquired with an Olympus 40x, 0.8 numerical aperture objective at 512 pixels × 512 pixels resolution. For fast-scanning volumetric imaging *in vivo* (Extended Data Figure 2G), the laser was directed through an 8 kHz resonant scanning galvonometer and the objective was controlled by a piezo-electric Zfocus.

Image Processing

All image processing was performed using custom scripts in Matlab or FIJI/ImageJ (NIH). Compartment (DAN subpopulation)-specific activity was computed by averaging all fluorescence signal within a manually defined MB γ lobe compartment. All DAN>sytGCaMP6s signals are normalized (divided) by MB247(KC)>dsRed fluorescence within the same ROI. Data from all other functional imaging experiments are plotted as raw fluorescence on an arbitrary scale or normalized as indicated.

Tethered Locomotion

For tethered locomotion experiments, a spherical treadmill was designed based on previous studies[53]. Briefly, a 6.35 mm diameter ball was shaped from Last-A-Foam FR-4618 (General Plastics) by a custom-made steel concave file. The ball rested in an aluminum base with a concave hemisphere 6.75 mm in diameter with a 1mm channel drilled through the bottom and connected to an airflow. The ball was recorded at 60–61 fps using a Point Grey Firefly Camera (Firefly MV 0.3 MP Mono USB 2.0, Point Grey, FMVU-03MTM-CS) with Infinity Lens (94mm focal length) focused on the ball while being illuminated by infrared LED lights. Ball rotation was calculated in real time using FicTrac software[54] running on computers with ≥3GHz processors speeds.

Closed-loop arena

The heading of the fly, as calculated by FicTrac, was transmitted to an Arduino Mega via serial port. Custom Arduino code was used to translate heading into tube position

controlled by motors described below. The closed-loop air-delivery system was custom designed using OnShape (www.onshape.com) and 3D printed using Visijet Crystal material at XHD resolution in a 3DSystems Projet 3510 HD Plus. O-ring OD and ID Gland surfaces were designed with excess material for printing then manually modified on a lathe for improved RMS [surface] finishing. 360° tube rotation was driven by a bipolar stepper motor (Pololu item #1206) controlled through a A4988 Stepper Motor Driver Carrier (Pololu #2980) coupled by a Dust-Free Timing Belt XL Series, 1/4" Width (McMaster-Carr, 1679K121, Trade No. 130×L025) to the rotating tube system, which rotated mounted on an Ultra-Corrosion-Resistant Stainless Steel Ball Bearing (3/4" Shaft Diameter, 1–5/8" OD, Mcmaster-Carr 5908K19). Air channel was kept airtight using oil resistant o-rings (1/16 Fractional Width, Dash Number 020, Mcmaster-Carr 2418T126). Motor rotation was measured by a rotary encoder (CUI Inc., AMT10 Series) that was used to correct for skipped steps.

Odor stimulation and airflow

Odor stimulation was achieved by directing a continuous stream of either 100 mL/min (low airflow conditions) or 400 mL/min (high airflow conditions) of clean air through a 2 mm diameter tube made of Visijet Crystal material directed at the fly's antenna. 10–20% of the total airstream was diverted through the headspace of a 500 mL bottle containing water. At a trigger, a custom-built solenoid valve controller system redirected the odor stream from the water bottle to a bottle containing the odorant, Apple Cider Vinegar (ACV, Heinz).

Sugar Feeding

For recordings involving sucrose, flies were tethered for imaging and locomotion as described above. Early during recovery from anesthesia, flies would often fully extend their proboscis before regaining other motor functions and at this point, glue was applied to the lateral sides of the proboscis with care taken to avoid glue contacting the distal proboscis, mouth parts, antennae, and aristae. As in all other tethered experiments, muscle 16 and obstructing trachea were removed with extra care taken to keep the antennal nerves and the esophagus intact. This approach allowed for flies to ingest sugar through their proboscis with minimal motion of the brain relative to the imaging plane. As a control for movement artifact in experiments recording GCaMP activity from all MB DANs, the stable fluorophore dsRed was expressed in the anatomically overlapping population of KCs and all DAN>sytGCaMP6s signals were normalized (divided) by MB247(KC)>dsRed fluorescence within the same ROI. In addition, this channel was monitored for movement artifact and trials that demonstrated changes in activity during sugar feeding beyond the range observed during spontaneous locomotion were excluded from analysis. For CNMF analysis of MB312B and MB316B flies (Extended Data Fig. 2A–D), occasional frames during sugar feeding demonstrated large movement artifacts. These frames were manually excluded and the neural activity at these timepoints was inferred using linear interpolation. For sucrose delivery, tethered flies were presented with nanoliter volumes of 1M sucrose via a Nanoject II Auto-Nanoliter Injector (Drummon, Cat. No. 3–000-204) positioned with a motorized micromanipulator (Scientifica). Red food coloring was added to the sucrose and the fly abdomens were inspected after each experiment to confirm sucrose ingestion.

Freely Moving Fly Behavior and Optogenetic Perturbations

Behavior in freely moving flies was assayed in a custom-built apparatus as described previously[28].

Data Analysis and Presentation

Unless otherwise noted, all analyses, visualizations, representations, normalizations, and averaging of behavior and DAN activity were performed or generated using custom scripts in Matlab and/or ImageJ. The following Matlab functions were used to generate the parenthetical variables/images: *imagesc* (heatmaps), *movcorr* (running correlations), *hist* (histograms), *kmeans* (k-means clustering). All figures, illustrations, schematics, and cartoons were created using Adobe Illustrator CC.

To facilitate visual comparison of neural activity and behavior (Figures 1C–E, 2A–C, 3B, 4A, Extended Data Figure 1F, 2, 3A,B,C,F, 4A–C, 8A, and Supplementary Fig. 3A–C,E) the behavioral variables of net motion and/or forward velocity were convolved by the biexponential rise and decay function of GCaMP6s (rise $t_{1/2}$=175 ms and decay $t_{1/2}$=550 ms), GCaMP6f (rise $t_{1/2}$=50 ms and decay $t_{1/2}$=150 ms), dLight (rise $t_{1/2}$=10 ms and decay $t_{1/2}$=100 ms), or jRGECO (rise $t_{1/2}$=40 ms and decay $t_{1/2}$=200 ms) and then multiplied by the mean of the top 10% of unconvolved behavioral variables for each trace (translated from radians/sec into mm/s according to the radius of the treadmill). In all other analyses the unconvolved behavioral data was used, as smoothing out the fine temporal structure of the signal could lead to the loss of relevant information within the data and introduce spurious temporal shifts.

Behavioral variables were captured at 60–61 frames/second while neural activity (fluorescence) was captured at 10 frames/sec. Due to electronic delays within the imaging system, however, frames were captured over a range of every 95–110 ms, creating irregular time stamps. To align these two distinct time-series, a standardized and regular time-series was generated for each trace containing 100 ms time bins (0, 100, 200, 300, etc.…). All behavioral or fluorescence data captured between these standardized cutoff points were averaged and assigned to the lower bound of the time bin. This allowed for neural and behavioral data to be aligned and meaningfully compared.

Comparisons of movement- and reward (sucrose)- related DAN activity and neurotransmitter release (Extended Data Figure 1B) were made by averaging normalized ($\Delta F/F_o$ with F_o = median trial fluorescence) sytGCaMP6s or dLight1.3b fluorescence during bouts of movement or during ingestion of 1M sucrose solution manually identified by concurrent digital video recording.

CNMF analysis was performed as follows: Frames with large motion artifacts were manually removed from the imaging stack, which was then motion corrected using non-rigid motion correction (NoRMCorre)[55]. ROIs were extracted using constrained non-negative matrix factorization (CNMF)[56]. Greedy and graph NMG initialization methods were used to extract ROIs corresponding to DAN presynaptic terminals and mushroom body compartments.

Anatomic reconstructions of γ4 DAN subpopulations (Extended Data Figure 1D) and γ4 DAN pre-synaptic boutons (Extended Data Figure 1E) were performed as follows: Using the female adult hemibrain, we analyzed the γ4 DAN subtypes PAM07, PAM08a, PAM08b, PAM08c, PAM08d, PAM08e. We screened driver lines corresponding to γ4 DAN subtypes using Neuronbridge[57]. γ4 DANs could be coarsely separated into neurons whose contralateral processes cross the midline over an upper commissure, which is covered in part by MB312B, or a lower commissure which is covered in part by MB316B. Presynaptic terminals corresponding to upper and lower commissure γ4 DANs were analyzed using neuPrint[58]-python (https://github.com/connectome-neuprint/neuprint-python) and plotted using navis (https://github.com/schlegelp/navis).

Instances of movement initiation (Figure 2B, Extended Data Figure 3A–F, Supplementary Figure 1) were identified *in silico* using a custom Matlab script that relied on a manually set cutoff to find inflection points in net motion after a prolonged pause (≥2 sec) followed by sustained movement (≥3 sec). Triggered average of parameters of behavior at the start of movement were normalized by dividing them by their average value during a given trial. Each individual behavioral trace was then aligned to generate the average, standard deviation, and 95% confidence interval and plotted on an arbitrary scale on an aligned set of axes. Relationships between DAN activity and different behavioral variables and relationships between different DANs during individual bouts of movement initiation were calculated by averaging the $\Delta F/F_0$ signal over the period of t=1 to t=2.5 seconds relative to the onset of movement and averaging the behavioral variables (normalized as above by division by their average value) over the relevant time period. Net motion, forward velocity, and |angular velocity|: t=1 to t=3. |Lateral velocity|: t=0 to t=1. Proportion of time moving after start is calculated over a 10 sec period after initiation of locomotion.

Principal component analysis (PCA) of behavioral variables during movement onset (Supplementary Fig. 1) was performed on the concatenation of net motion, forward velocity, |angular velocity|, and |lateral velocity| across a 4 second time window centered on instants of movement initiation (4 variables × 4 sec time window × 10 Hz sampling = 160 initial variables per start). All behaviors were z-scored over the 4 sec window prior to concatenation.

To identify bouts of movement and periods of quiescence, custom Matlab scripts used manually set cutoff values and the non-convolved net-motion recordings to perform an *in silico* identification of periods of walking and periods of not walking during trials. Walking/still designations were then manually verified and time points of transition stored to be used in subsequent analyses.

Probability of accurate walking state prediction (Figure 2C) was calculated as follows:

Epochs of movement and quiescence were identified as above. All data from a single animal were concatenated and 20% of time points were randomly set aside (using Matlab function *randperm*) while the remaining 80% were used to train a multinomial logistic regression model (*mnrval*) to predict locomotor state from compartmentalized DAN activity. The model was then tested on the previously allocated 20% of time points. During testing, the model

produced both a prediction of locomotor state and probability of accuracy. Predictions were compared with actual locomotor state and the probability of accuracy of correct predictions were averaged (with incorrect predictions assigned a value of zero). This process was repeated 100 times for each animal and the mean probability of accurate predictions was averaged across all 100 repetitions.

Increases in forward velocity and |angular velocity| (Extended Data Figure 4B,C) were calculated as follows:

A custom Matlab script isolated local maxima in forward or |angular| acceleration during bouts of movement and the preceding point of acceleration=0 was then identified, and velocity and neural activity were then aligned to these time points. To exclude instances when animals altered both their forward and angular velocities, epochs in which the acceleration of the alternative behavioral variable rose beyond a manually set cutoff point were excluded. For plotting, behavior centered on these inflection points were z-score normalized by the average behavior over a time window from t=−2 to t=2. Neural activity was plotted as $\Delta F/F_o$ with F_o defined as neural activity from t=−1 to t=0. Behavior and neural activity were then aligned to generate the average and standard deviation of the given variable.

Linear filters were fit using standard linear regression in which the least squared error between true and predicted output was minimized to identify best-fit filters. Specifically, for a given DAN variable x (e.g., $\gamma 4$) and behavioral variable y (e.g., forward velocity), we let the estimate y*(t) of behavior at time t be given by $y^*(t) = a(-\tau)x(t-\tau) + a(-\tau+\Delta t)x(t-\tau+\Delta t) + ... + a(\tau-\Delta t)x(t+\tau-\Delta t)$. We then found the $a(-\tau)$, ..., $a(\tau-\Delta t)$ that minimized the squared difference between y(t) and y*(t), averaged over all t within a given trial. Only timepoints during which the animal was walking were used in the fitting procedure. All filter fitting was performed using the scikit-learn package in Python.

The proportion of DAN variance explained by specific behavioral variables (Figure 2F) was calculated using an adjusted R^2 value, ($R^2_{adj} = 1 - (1 - R^2)(n-1)/(n-p-1)$, where n is the number of valid timepoints used in the filter fit (i.e., the number of timepoints where the fly was locomoting), and p is the number of time points (free parameters) in the linear filter. This quantity adjusts for spurious increases in standard R^2 due to a large number of free parameters relative to data points. We chose this metric because it allowed us to capture individual variation in DAN variance explained by behavior across flies and trials without requiring us to hold out data for cross-validation (since many trials did not have sufficient data points to do so due to the limited amount of time the fly was walking). Negative R^2 values, which largely reflect a scarcity of data in an individual trial, were not plotted.

Predictions of behavioral variables from single and all DAN compartments (Extended Data Figure 4G) were made by fitting linear filters to 80% of trials and evaluating them on the held-out 20% of trials. Filters were defined as the best-fit weights in a weighted sum of either one or all DAN activity levels in the 8 seconds surrounding the timepoint of the behavior to be predicted (e.g., for single DANS imaged at 10 Hz, there were 80 weights to fit, and for all 4 DANS, 320 weights to fit). All trials used in fitting were aggregated

before fitting due to the large number of weights in the 4-DAN filter, with a random 80/20 fitting/test split of trials repeated 50 times. For each split, filter weights were chosen to be those that minimized the squared difference between the true and predicted behavioral variable, averaged over all timepoints in all trials used for fitting. Filters were evaluated by calculating the R^2 between the true and filter-predicted behaviors in the 20% of held-out trials.

Partial correlations (Extended Data Figure 4F) were generated via custom Python scripts in the following way. To calculate the partial correlation between two variables x and y, conditioned on auxiliary variables $z_1, z_2, ...$, we first computed the best fit linear predictions x^* and y^* for x and y, respectively using $z_1, z_2, ...$, as the only predictors (in addition to an intercept term). The partial correlation between x and y given $z_1, z_2, ...$, was then computed as the Pearson correlation between $(x - x^*)$ and $(y - y^*)$. Both the net ball motion signal and the other DAN activities were included in the auxiliary variables.

Position of tethered flies on a fictive 2-dimensional plane was calculated by FicTrac software based on the diameter of the foam ball upon which the fly was walking, and representations of fictive walking trajectories were generated using custom written Matlab scripts.

Neural activity and behavior at odor onset were identified using the aligned internal timestamps generated with Bruker Nanosystems software or FicTrac software, respectively, and representations were generated using custom written Matlab scripts. For DAN activity, $\Delta F/F_o$ was calculated with F_o defined as the average normalized (see *Image Processing*) GCaMP fluorescence during a 10 second period immediately prior to odor onset. In air controls were similarly calculated except with a 15-second temporal offset.

Individual odor responses were aggregated from trials across multiple flies. Every fly was presented with at least 10 odor presentations, but trials in which FicTrac failed to continuously track the fly's movements throughout the period immediately preceding and through the entire odor presentation were excluded, as in these instances the animal was not maintained in the closed-loop virtual reality configuration. As a result, the number of trials from any individual fly included in the dataset ranged from 3 to 12. We therefore aggregated responses across animals to examine the relationship between changes in DAN activity and changes in different behavioral variables.

Relationships between averaged DAN activity and behavior during an odor trial were calculated as follows:

Upwind displacement was divided by the individual fly's average walking speed in the 10 seconds prior to odor presentation and then calculated as the change in fictive position along the axis of airflow from the start of the odor plume (t=0) until the end of the odor plume (t=10). Changes in forward velocity or |heading| were calculated by subtracting the average forward velocity or |heading| during bouts of movement in the 10 second period preceding odor onset (t=−10 to t=0) from the average forward velocity or |heading| during bouts of movement occurring within the odor plume (t=2 to t=10, to account for any delays in odor delivery). Using shorter or longer time bins gave similar results. γ DAN $\Delta F/F_o$

was averaged over t=2 to t=10 sec after odor onset with F_o= average sytGCAMP6s activity during bouts of movement from t=−10 to t=0 seconds before the onset of odor. Relationships between averaged DAN activity and behavior as animals walked in clean air (Extended Data Figures 5A,B,E,F) were calculated similarly except over the 20 seconds preceding an odor stimulus. Subsampling of odor responses (Extended Data Figure 5H,I) was performed by serially excluding data below or above a manually set cutoff point until the variances of the behavioral variables in the two datasets was approximately equal.

Linear Model (Figure 3E, 4C, 5 and Extended Data Figures 6, 9):

Prior to filter fitting we z-scored normalized DAN activity within each compartment relative to the entire 5-minute trial. Forward velocity was normalized by dividing all timepoints by the median forward velocity computed during all identified walking periods in the trial. Absolute (unsigned) heading was measured in radians. We then considered either the 10 seconds prior to odor onset (in air) or the 10 seconds following odor onset (in odor). The average 10-second activity of each DAN subset across all trials was then subtracted from the DAN activity during each individual trial (either in or out of odor) to account for any rapid rise or fall during odor onset and allow the filters to better explain how behavior gives rise to the fluctuations around the mean response. Using the collection of 10-second windows aggregated across all odor pulses and trials for either the “in odor” or “in air” period we then fit 5-second linear filters predicting DAN activity from the two behavioral variables. Specifically, for each compartment we assumed DAN activity at time t, g(t), was a weighted sum of the forward velocity and absolute heading signals in a window extending 4 seconds prior to t and 1 second after. Mathematically, we let the estimate

$$g^*(t) = w^h_{-4}h(t-4) + w^h_{-3.9}h(t-3.9) + \ldots + w^h_{0.9}h(t+0.9) + w^h_{1}h(t+1) + w^v_{-4}v(t-4) + w^v_{-3.9}v(t-3.9) + \ldots + w^v_{0.9}v(t+0.9) + w^v_{1}v(t+1)$$

where h and v are absolute heading and forward velocity, respectively. We chose all w’s by minimizing the squared error $(g(t) - g^*(t))^2$ averaged across time, pulses, and trials. This yielded 5 seconds of absolute heading and forward velocity weights for each DAN compartment in each period (“in air” and “in odor”). We repeated this process across all conditions (low-flow, high-flow, fed). Experimentally-derived data was similarly normalized when directly compared with model-generated data.

Cross correlation matrices (Extended Data Figure 7) were generated in Python in the following way. For each 10-second odor pulse across all trials, all measured variables (DAN activity, heading, etc.) within the 20 sec time window surrounding the pulse onset were selected and stored (i.e., the window included the 10 seconds prior to the pulse and the 10 sec of the pulse itself). For each variable this generated an initial data matrix with the number of rows equal to the number of odor pulses across all trials and with 200 columns (20-seconds x the 10 Hz sampling). DAN activity was normalized for each pulse by subtracting and then dividing by the average fluorescence within this 20-second window. Forward velocity and heading were normalized by subtracting the forward velocity or heading, respectively, averaged over the first 10 seconds (the 10 seconds preceding the odor pulse onset). A correlation matrix between variables *x* and *y* across odor pulses was

then generated by computing the Pearson correlations between $x(t_1)$ and $y(t_2)$ for all t_1 and t_2 spanning the 20-second window. P values were calculated as standard Pearson correlation p values using the scipy Python package.

The nested model analysis (Extended Data Figure 8) used linear models and significance levels for the increase in variance explained (as stepwise predictors were added) were computed using an F-test. Models were fit and analyzed using Python scripts and results were plotted in Matlab. Briefly, for a given condition (low or high airflow) and DAN compartment, each odor pulse was treated as a "trial". Across trials, we sought to predict DAN activity during the initial phase of odor presentation (γ_{1-4}, time-averaged 1–4 seconds post odor onset) using combinations of the following predictors: |heading| time-averaged over the 10 sec prior to odor onset (h_o), initial Δforward velocity (time-averaged from 1–4 sec post odor onset, Δv_{1-4}), initial Δ|heading| (time-averaged from 1–4 sec post odor onset, Δh_{1-4}), and future Δ|heading| (time-averaged from 7–10 sec post odor onset, Δh_{7-10}). Windows were chosen based on the approximately 3-second heading autocorrelation time. We then proceeded with a stepwise regression: for a given condition and DAN compartment we first identified (using least-squares regression) the best linear prediction of initial DAN activity (γ_{1-4}) given h_o alone. That is, we identified the parameter a in the model $g^* = ah_o$ that minimized $(\gamma_{1-4} - \gamma^*)^2$ averaged over all trials/pulses. We next added initial forward velocity as a predictor by identifying the best-fit parameters a, b in the model $\gamma^* = ah_o + b\Delta v_{1-4}$ and recomputed the trial/pulse-averaged error. We repeated the procedure by sequentially adding in the remaining two predictors Δh_{1-4} and Δh_{7-10} and recomputing the corresponding error. This stepwise regression allowed us to evaluate whether the predictive power gained by adding in each new predictor was significant by comparing the explained variances of the model with and without the candidate predictor using an F-test.

Statistical analysis

All statistical analyses were performed using built in Matlab functions unless otherwise noted. Exact p values for every statistical test performed is listed in Supplementary Table 2.

Pearson Correlation Coefficient and associated p-value: *corrcoef*

One-way ANOVA followed by Tukey's multiple comparison test: *anova1* and *multcompare*

Fisher r-to-z transformation was calculated using http://vassarstats.net/rdiff.html

2-tailed paired t-tests with Holm-Bonferroni post-hoc correction: *ttest*

Unpaired t-tests with Holm-Bonferroni post-hoc correction: *ttest2*

Two-sample F-test for equal variances: *vartest2*

Extended Data

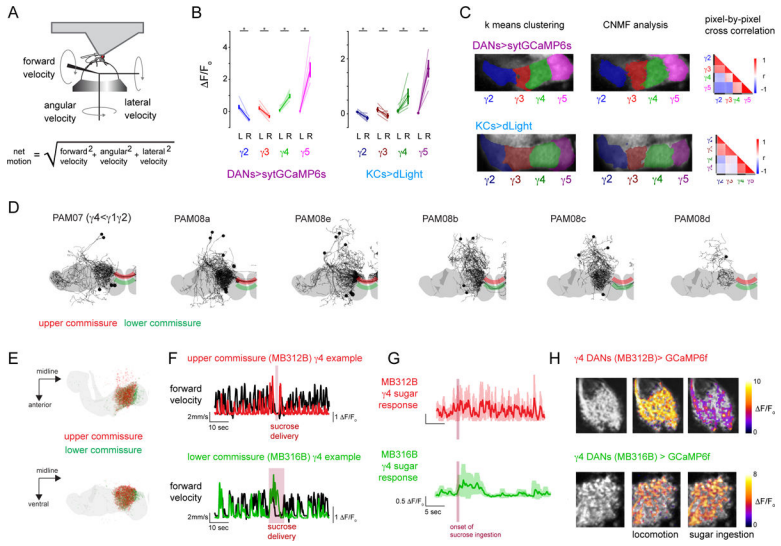

Extended Data Fig. 1. Compartmentalized DAN activity and dopamine release coordinately represent reward and locomotion.

(A) Schematic depicting experimental system and definition of the quantified parameters of locomotion. **(B)** Comparison of maximum DAN activity measured by sytGCaMP6s expressed in DANs (left) and dopamine release measured by dLight expressed in Kenyon cell (KCs) (right) in response to ingestion of a sucrose reward (R) or during locomotion (L). Signals normalized by subtracting the median fluorescence during the 5 min trial. Paired two-sided t-test with Bonferroni correction, $p<0.05$(*), see Supplementary Table 2. **(C)** Correlated and compartmentalized sytGCaMP6s activity in γ lobe DANs (top) and KC dLight expression reflecting dopamine release (bottom) during periods of spontaneous locomotion and sucrose ingestion. Multiple clustering algorithms identify each compartment as a relatively homogenous unit, with stronger correlations within than across compartments. Left: pixels color coded by k-means clustering analysis. Middle: pixels color coded by CNMF clustering analysis. Right: pixel-by-pixel cross-correlation (Pearson correlation coefficient) for the same animal. **(D)** Anatomic reconstructions of γ4 DAN subpopulations from hemibrain connectome. Upper and lower axonal commissures that DANs use to innervate the lobes highlighted in red and green, respectively. **(E)** Presynaptic distribution of DANs following upper (red) and lower (green) commissure within the γ4 compartment. **(F)** Overlay of forward velocity (black) and activity of either the MB312B+ γ4 DANs (top, which follow the upper commissure, red) or MB316B+ γ4 DANs (bottom, which follow the lower commissure, green) expressing GCaMP6f during locomotion and sucrose ingestion (maroon bar). **(G)** Average MB312B (top, upper commissure, red) or MB316B (bottom, lower commissure, green) responses aligned to the beginning of sucrose ingestion (maroon bar). N for MB312B= 6 animals, 10 sucrose presentations. N for MB316B= 5 animals, 14 sucrose presentations. **(H)** Heat map of maximum $\Delta F/F_o$ for MB312B (top, upper commissure) or MB316B (bottom, lower commissure) during locomotion (middle) or sugar ingestion (right) overlaid on GCaMP fluorescence (left) highlights that MB312B+

DANs are active during locomotion but not reward ingestion while MB316B+ DANs display multiplexed activity during both contexts.

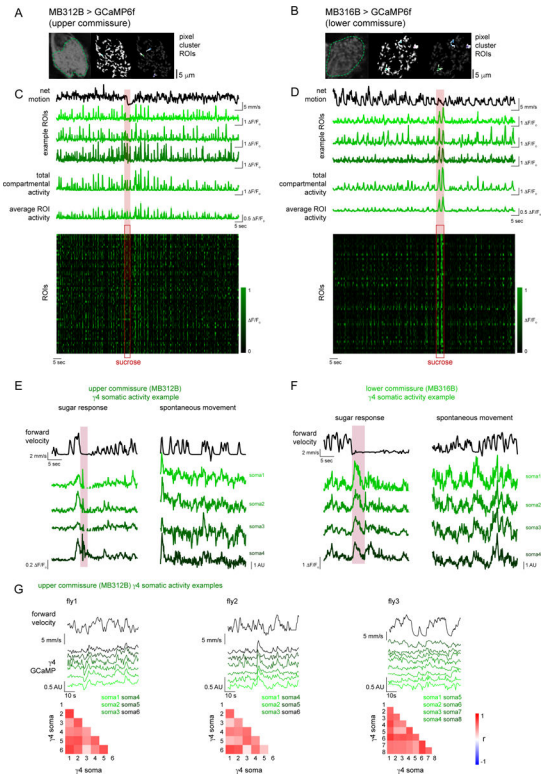

Extended Data Fig. 2. Multiplexed and correlated activity in γ4 DAN subsets.

(A) MB312B+ γ4 DANs (upper commissure) expressing GCaMP6f fluorescence (left) with functionally correlated and spatially adjacent pixels clustered into single ROIs by CNMF analysis (middle). Right: representative ROIs whose activity is plotted in (C). Similar results observed in N=6 animals. **(B)** Same as in (A) but for MB316B+ γ4 DANs (lower commissure). Right: representative ROIs plotted in (D). Similar results observed in N=5 animals. **(C)** Net motion (top row, black) aligned to the activity in representative CNMF-generated-ROIs from (A) (2nd, 3rd, and 4th rows, shades of green), total MB312B+ DAN GCaMP activity (5th row), the average CNMF-generated-ROI activity (bottom row), and the activity in all ROIs (heatmap) from a representative experiment in a MB312B>GCaMP6f individual. Maroon bars indicate period of sucrose ingestion. **(D)** As in (C) but for MB316B+ γ4 DANs (upper commissure). Maroon bars indicate period of sucrose ingestion. **(E)** Cytoplasmic GCaMP6f activity in MB312B+ γ4 DAN soma (shades of green) in representative examples during sugar ingestion (left) and spontaneous movement (right) aligned to forward velocity (top row, black). Different shades of green indicate different γ4 DAN soma recorded from the same animal. Maroon bars indicate period of sucrose ingestion. **(F)** As in (E) but recording from MB316+ γ4 DAN soma. **(G)** Motor-associated signals across individual γ4 DANs is highly correlated. Cytoplasmic GCaMP6f activity in MB312B+ γ4 DAN soma measured with volumetric imaging during spontaneous bouts of locomotion. For three flies: top row shows a representative bout of forward velocity (black), middle row shows cytoplasmic GCaMP6s fluorescence (shades of green indicate different

γ4 DAN soma), and bottom row is heatmap depicting the cross-correlation (Pearson correlation coefficient) between GCaMP6s signals in different γ4 DANs during spontaneous locomotion in a 5 min trial.

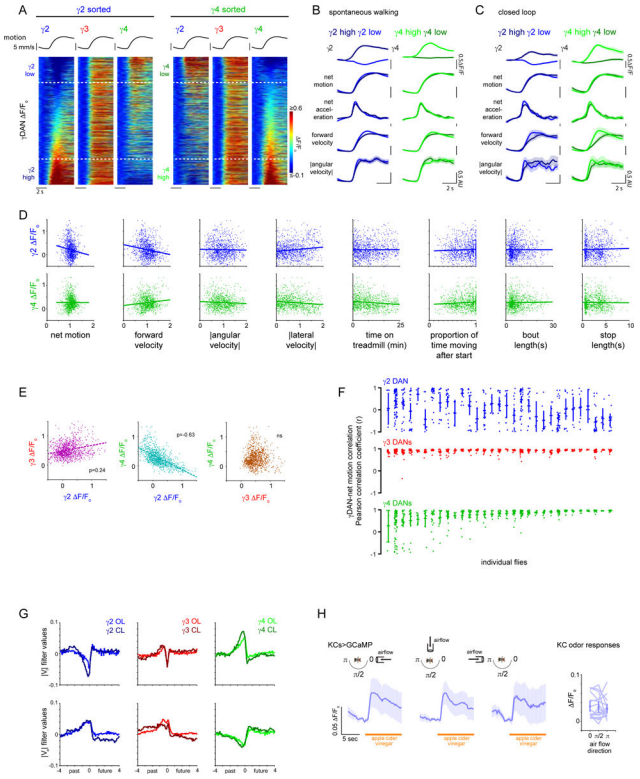

Extended Data Fig. 3. Variability of DAN - behavior correlations.

(A) Top: average motion (black) ± 95% confidence interval (CI, obscured by average line) as animals initiate locomotion. Bottom: heat map of $\Delta F/F_o$ in γ DANs aligned to movement initiation. Rows (bouts) ordered by average γ2 (left) or γ4 (right) $\Delta F/F_o$. Dashed lines indicate 20% of trials with highest or lowest average $\Delta F/F_o$. N=53 animals, 1060 starts. **(B)** DAN activity and parameters of locomotion during spontaneous movement initiation in which γ2 and γ4 were most differentially active). Left: average γ2 $\Delta F/F_o$ (top), motion (2nd row), acceleration (3rd), forward velocity (4th), and |angular velocity| (bottom) ± 95% CI as animals initiated locomotion. 20% of bouts of movement initiation with highest (dark) and lowest (lighter) average γ2 $\Delta F/F_o$ as indicated by lines in (A). Right: as left but for with highest (ligher) and lowest (dark) average γ4 $\Delta F/F_o$. N=212 bouts. **(C)** As in (B) but for flies walking in non-odorized air in closed-loop. N=91 bouts. **(D)** γ2 (top) and γ4 (bottom) DAN activity vs different behavioral variables. N=1060 bouts. All Pearson correlation coefficients are either weak (|r|<0.18) or not significant (no Bonferroni correction). **(E)** Comparisons of average DAN $\Delta F/F_o$ during the onset of locomotion. Pearson correlation coefficient (r) indicated where relationship is statistically significant (p<0.00001, Bonferroni correction, see Supplementary Table 2). N=1060 starts. **(F)** Pearson correlation coefficient between change in DAN activity and net motion during bouts of movement initiation for flies walking in clean air in closed-loop. Columns (flies) ordered by average γ4-motion correlation. N=32 animals, 452 starts. **(G)** Filters predicting DAN activity from forward

velocity (top) or |angular velocity| (bottom) in open loop (OL, as in Figure 1F, light lines) or closed-loop (CL) in clean air. ± 95% CI. OL: N=66 animals, 119 5-minute trials. CL: N=20 animals, 32 5-minute trials. **(H)** Comparison of γ Kenyon Cells activity during presentation of apple cider vinegar from indicated angles. Average $\Delta F/F_0$ (dark line) ± 95% CI aligned to odor onset. Right: average $\Delta F/F_0$ during odor presentation from indicated angles. N=16 animals, 3 odor presentations per orientation (total 144 odor presentations). One-way ANOVA followed by Tukey's multiple comparison test; no statistical significance observed.

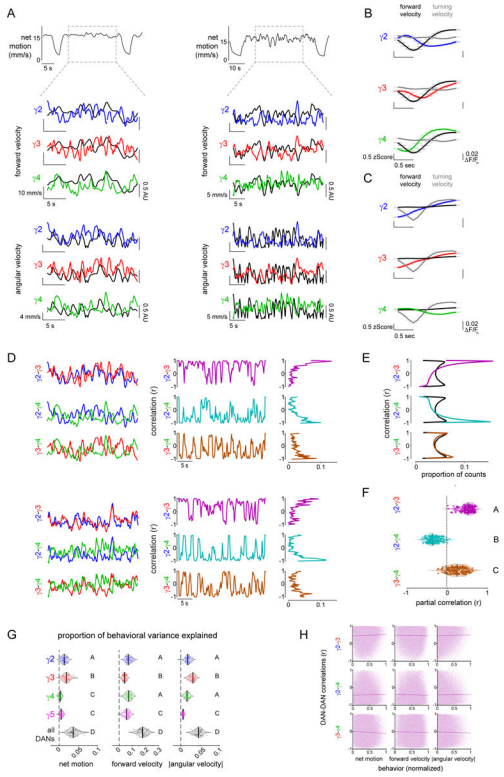

Extended Data Fig. 4. Rapidly fluctuating network correlations between DANs and different behavioral variables.

(A) Representative traces from two flies showing the net motion of each animal (top), overlay of γ DAN activity (colored) and either forward velocity (middle rows, black) or turning velocity (bottom rows, black) during a period of continuous locomotion (epoch shown by gray dashed box in top trace). DAN activity is normalized to minimum and maximum values during the selected bout of walking. **(B)** Average activity of γ DANs aligned to increases in forward velocity during bouts of continuous movement. N=9,772 movements in 74 flies. **(C)** Average activity of γ DANs aligned to increases in turning velocity during bouts of continuous movement. N=11,667 movements in 74 flies. **(D)** Left: overlay of DAN activity in different compartments during epochs designated in (A). Top: same epoch as left panel of (A). Bottom: same epoch as right panel of (A). Middle: running cross-correlation between pairs of γ DANs for the traces at left. Right: histograms of running correlation. **(E)** Histogram of running cross-correlation between pairs of γ DANs for all flies. Shuffled controls (random 1–20 sec temporal shift) in black. N=74 animals,

178 5-minute trials. **(F)** Partial correlations between γ DANs to control for potential relationships that arise from common behavioral signals. N=74 animals, 178 5-minute trials. ANOVA followed by Tukey's multiple comparison test with. Data labeled with different letters are significantly different from each other ($p < 0.00001$). **(G)** Proportion of the variance (R^2) in net motion (left), forward velocity (middle), and |angular velocity| (right) explained by individual and all DANs. N=66 animals, 119 5-minute trials. ANOVA followed by Tukey's multiple comparison test. Data labeled with different letters are significantly different from each other ($p < 0.0005$). **(H)** No significant relationships are apparent between intercompartmental correlations and behavioral parameters. Pearson correlation coefficient between pairs of γ DANs and different parameters of movement during bouts of continuous locomotion. All Pearson correlation coefficients are either weak ($|r|<0.1$) or not significant, see Supplementary Table 2. p values not adjusted with Bonferroni correction.

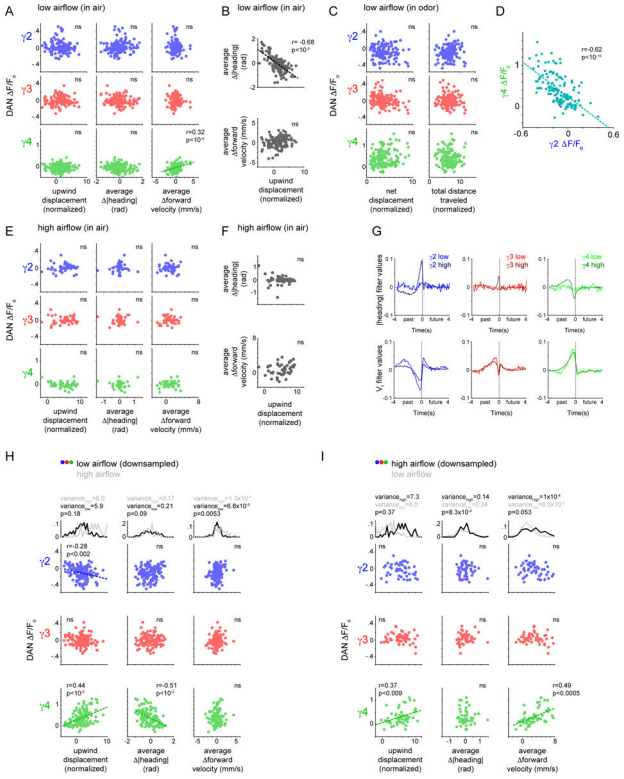

Extended Data Fig. 5. DAN-motor correlations vary across conditions.

(A) Same analysis as in Figure 3F but offset by 15 sec such that animals were walking only in clean air. N=26 flies, 143 epochs. **(B)** Same analysis as in Figure 3C but offset by 15 sec such that animals were walking in clean air. Fisher r-to-z transformation indicates no significant differences. in correlation coefficients between upwind displacement and Δ|heading| in and out of odor ($z=-1.32$). N=26 flies, 143 odor presentations. **(C)** Average γ DAN $\Delta F/F_0$ shows no correlations with an animal's net displacement (left) or total scalar distance traveled (right) during odor presentations. Displacement was normalized (divided by) an individual's average walking speed. Pearson correlation coefficient (r) indicated where relationship is statistically significant ($p=10^{-15}$, Bonferroni correction). N=26 flies, 143 epochs. **(D)** $\Delta F/F_0$ of DANs in the γ2 vs γ4 compartments during odor

presentation. Pearson coefficient (r) indicated where relationship is significant ($p<0.0001$, see Supplementary Table 2). N=26 flies, 143 odor presentations. **(E)** Same analysis as in Figure 4D but offset by 15 sec such that flies were walking in clean air. N=22 flies, 52 odor presentations. **(F)** Same analysis as in Figure 4B but offset by 15 sec such that animals were walking in clean air. N=22 flies, 52 odor presentations. **(G)** Filters predicting DAN activity from |heading| (top) or forward velocity (bottom) as animals walked in clean air, under low (lighter) or high airflow (darker) conditions. ± 95% confidence interval obscured by thickness of the data line. **(H)** Average γ DAN $\Delta F/F_o$ plotted as a function of upwind displacement (left), Δ|heading| (middle), and Δ forward velocity (right) during odor presentation from Fig. 3F however here data from the low airflow context was subsampled such that the variance of the Δ |heading| was statistically equal to that of the high airflow context. Top: distribution of range of behavior. Pearson coefficient (r) indicates where relationship between subsampled variables is significant ($p<0.05$ with Bonferroni, see Supplementary Table 2). N_{low} airflow=135 odor presentations. **(I)** Same as (H) except when data from the high airflow context is subsampled such that the variance of the Δforward velocity was statistically equal to that of the low airflow context. N_{high} airflow=50 odor presentations.

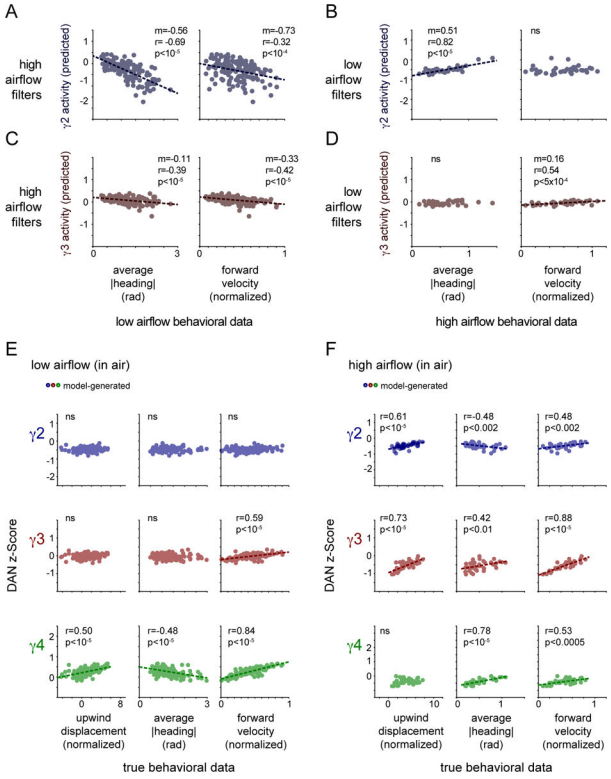

Extended Data Fig. 6. Analysis of dynamic DAN-motor correlations.

(A) Average predicted γ2 odor responses generated from high airflow filters plotted as a function of upwind displacement (left), |heading| (middle), and forward velocity (right) during odor presentation under low airflow conditions. Best fit line and Pearson coefficient (r) indicated where relationship is significant ($p<0.0001$, Bonferroni correction, see Supplementary Table 2). N=26 flies, 143 odor presentations. **(B)** As in (A) but predicted

DAN odor responses generated from low airflow filters plotted against behavior under high airflow conditions. Best fit line and Pearson coefficient (r) indicated where relationship is significant ($p<0.0001$, Bonferroni correction). N=22 flies, 52 odor presentations. **(C-D)** Same as (A-B) except for γ3 DAN odor responses. N=26 flies, 143 odor presentations (C), N=22 flies, 52 odor presentations (D). **(E)** Average predicted DAN odor responses plotted as a function of upwind displacement (left), |heading| (middle), and forward velocity (right) as animals walked in clean air, under low airflow. Best fit line and Pearson coefficient (r) indicated where relationship is significant ($p<0.01$ with Bonferroni correction, see Supplementary Table 2). N=26 flies, 143 odor presentations. **(F)** Same as (A) except under high airflow. N=22 flies, 52 odor presentations.

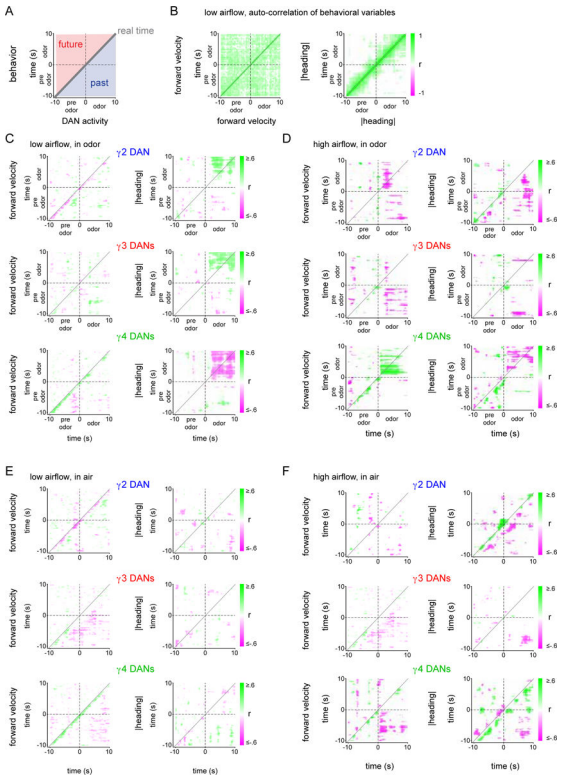

Extended Data Fig. 7. Cross-correlation analysis between DAN activity and behavior during odor pursuit.

(A) Organization of cross correlation matrix comparing DAN activity to past, present, and future behavior in and out of odor. **(B)** Auto-correlation of forward velocity (left) and |heading| (right) before and during odor presentation during the 10 sec prior to odor and the 10 sec of odor presentation. Colored points indicate statistically significant correlations (Pearson correlation coefficient, $p<0.05$, no Bonferroni correction, see Supplementary Table 2). N=26 flies, 143 odor presentations. Note the correlation between an animal's current and past or future forward velocity extend throughout the trial, while the correlation between an animal's current and past or future heading is < 3 sec. **(C-D)** Cross correlation matrix between forward velocity (left) or |heading| (right) and γ DAN activity during the 10 sec prior to odor onset and the 10 sec during odor presentation under low (C) and high (D) airflow conditions. Only relationships that are statistically significant by Pearson cross

correlation ($p<0.05$, no Bonferroni correction, see Supplementary Table 2) are shown in color indicated by green-magenta scale. N=26 flies, 143 odor presentations (C), N=22 flies, 52 odor presentations (D). **(E-F)** Same analysis as in (C-D) but over a 20-sec period during which only clean air is presented to the animal. Colored points indicate statistically significant correlations ($p<0.05$, no Bonferroni correction, see Supplementary Table 2). N=26 flies, 143 odor presentations (E), N=22 flies, 52 clean air epochs (F).

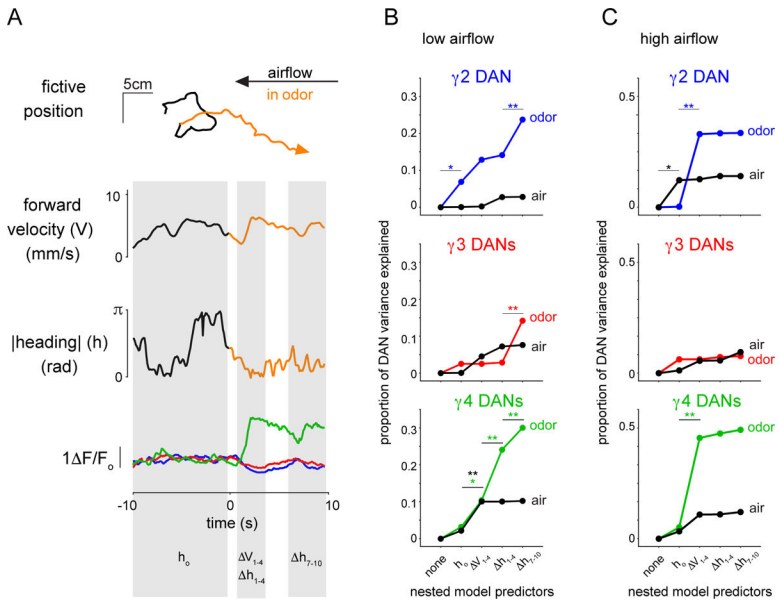

Extended Data Fig. 8. Correlations between DAN activity and current and future behavior emerge during odor tracking.

(A) Representative trial showing fictive 2D trajectory, forward velocity, |heading|, and γ DAN activity in which the fly reorients and tracks upwind in response to apple cider vinegar in the low airflow context. Black trajectories indicate clean air, orange indicates time of odor presentation. Shaded areas represent epochs used in nested linear model (B). **(B)** A nested linear model predicting γ DAN activity during the initial phase of odor presentation under low airflow conditions (t=1–4 sec after odor onset) based on an animal's average heading 10 sec prior to odor onset (h_o), initial Δforward velocity (t=1–4 sec, $\Delta V_{1–4}$), initial Δ|heading| (t=1–4 sec, $\Delta h_{1–4}$), and future Δ|heading| (t=7–10 sec, $\Delta h_{7–10}$, a time window when behavioral autocorrelations are no longer relevant). Fraction of DAN variance explained as a function of which predictors were included in the model, for odor presentation (colored lines) and same temporal epochs offset 10 sec prior to the odor presentation (black) when the fly walked in clean air. F-test, $p<0.05$ (*), $p<0.01$ (**) with colored asterisk depicting significant differences in odor and black asterisk depicting significant differences in clean air. N=26 flies, 143 odor presentations. **(C)** Same as (B) except under high flow conditions. N=22 flies, 52 odor presentations.

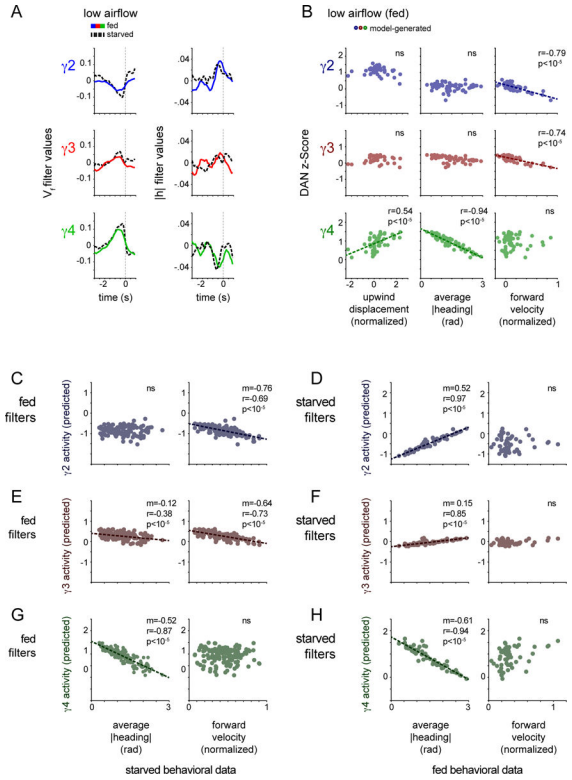

Extended Data Fig. 9. DAN-movement relationships during odor tracking in low airflow conditions are comparable in starved and fed animals.

(A) Linear filters predicting DAN activity using forward velocity (V_f, left) or |heading| (|h|, right) in fed (colored lines) and starved (black dashed lines) flies during odor tracking over a 4 second window. N=10 flies, 49–53 odor presentations. **(B)** Average predicted DAN activity plotted as a function of upwind displacement (left), |heading| (middle), and forward velocity (right) during odor presentation in fed individuals. Best fit line and Pearson correlation coefficient (r) indicated where relationship is statistically significant ($p<0.0001$ with Bonferroni correction, see Supplementary Table 2). **(C-D)** Average predicted γ2 DAN odor responses generated by applying filters derived from fed animals to behavioral data from starved (C) or fed (D) animals, plotted as a function of |heading| (left) or forward velocity (right) during odor presentation. Best fit line and Pearson correlation coefficient (r) indicated where relationship is statistically significant ($p<0.0005$ with Bonferroni correction, see Supplementary Table 2). N=10 flies, 49 (fed) and 53 (starved) odor presentations. **(E-F)** Same as (C-D) but for γ3 DANs. **(G-H)** Same as (C-D) but for γ4 DANs.

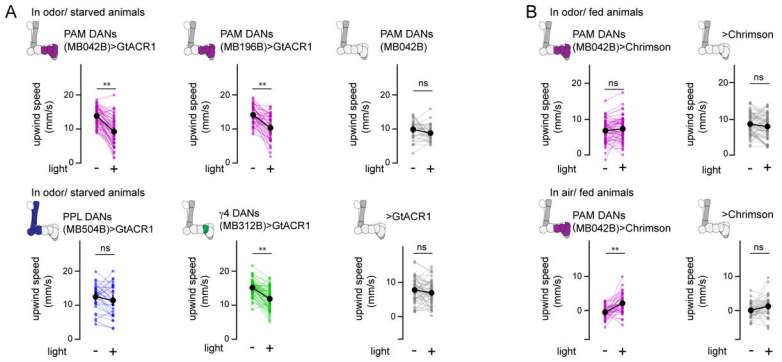

Extended Data Fig. 10. Optogenetic inhibition or excitation of PAM DANs bidirectionally influences upwind tracking behavior.

(A) Average upwind velocity during odor presentations preceding optogenetic inhibition (−) and during odor presentations paired with optogenetic inhibition (+) for the indicated genotypes in starved animals. PAM DANs (MB042B driver)>GtACR1 (N=63, top left), PAM DANs (MB196B driver)>GtACR1 (N=49, top middle), PAM DANs MB042B-Gal4 parental controls (N=33, top right), PPL DANs (MB504B driver)>GtACR1 (N=30, bottom left), γ4 DANs (MB312B driver)>GtACR1 (N=54, bottom middle), UAS-GtACR1 parental controls (N=48, bottom right). Paired two-sided t-test with Bonferroni correction, p<10–5 (**), see Supplementary Table 2. **(B)** Top: average upwind speed in odor presentations preceding optogenetic activation (−) and in odor predsentations paired with optogenetic activation (+) in fed PAM DANs (MB042B driver)>CsChrimson flies (left) and UAS-CsChrimson parental controls (right). N=60 paired cohorts of PAM>CsChrimson and parental control animals assayed together during a single experiment. Bottom: average upwind speed of fed animals in clean air preceding optogenetic activation (−) and with optogenetic activation (+) for fed PAM DANs (MB042B driver)>CsChrimson flies (left) and UAS-Chrimson parental controls (right). N=44 paired cohorts of PAM>CsChrimson and parental control animals assayed together during a single experiment. Paired two-sided t-test with Bonferroni correction, p<10–5 (**), see Supplementary Table 2.

Supplementary Material

Refer to Web version on PubMed Central for supplementary material.

Acknowledgements

We thank Sandeep Robert Datta, Barbara Noro, Annie Handler, and members of the V.R. lab for valuable discussion and comments on the manuscript; Chuntao Dan, Vivek Jayaraman, and Lin Tian for developing the dLight sensor flies, and Jim Petrillo and Patrick Stock for technical advice. Stocks from the Bloomington *Drosophila* Stock Center (NIH P40OD018537) were used in this study. This work was supported by National Institutes of Health (R01NS113103 and DP2NS087942 for V.R, T32GM007739 to the Weill Cornell/Rockefeller/Sloan Kettering Tri-Institutional MD-PhD Program for (A.Z. and A.S.), a Kavli Neural Systems Institute Fellowship (A.S.) and the Simons Collaboration on the Global Brain (V.R. and A.F.).

Data availability

The data that support the findings of this study are available at https://www.dropbox.com/sh/3cx7d3xw5qbsopi/AADPFcas9jq1Ev1i3FrKKwdDa?dl=0

Referenced Literature

1. Bargmann CI & Marder E From the connectome to brain function. Nat. Methods 10, 483–490 (2013). [PubMed: 23866325]
2. Schultz W, Dayan P, & Montague PR A neural substrate of prediction and reward. Science 275, 1593–1599 (1997). [PubMed: 9054347]
3. Watabe-Uchida M, Eshel N & Uchida N Neural Circuitry of Reward Prediction Error. Annu. Rev. Neurosci 40, 373–394 (2017). [PubMed: 28441114]
4. Waddell S Reinforcement signalling in *Drosophila*; dopamine does it all after all. Curr. Opin. Neurobiol 23, 324–329 (2013). [PubMed: 23391527]
5. Da Silva JA, Tecuapetla F, Paixão V & Costa RM Dopamine neuron activity before action initiation gates and invigorates future movements. Nature 554, 244–248 (2018). [PubMed: 29420469]
6. Howe MW & Dombeck DA Rapid signalling in distinct dopaminergic axons during locomotion and reward. Nature 535, 505–510 (2016). [PubMed: 27398617]
7. Panigrahi B et al. Dopamine Is Required for the Neural Representation and Control of Movement Vigor. Cell 162, 1418–1430 (2015). [PubMed: 26359992]
8. Salamone JD & Correa M The Mysterious Motivational Functions of Mesolimbic Dopamine. Neuron 76, 470–485 (2012). [PubMed: 23141060]
9. Beierholm U et al. Dopamine Modulates Reward-Related Vigor. Neuropsychopharmacology 38, 1495–1503 (2013). [PubMed: 23419875]
10. Parker NF et al. Reward and choice encoding in terminals of midbrain dopamine neurons depends on striatal target. Nat. Neurosci 19, 845–854 (2016). [PubMed: 27110917]
11. Engelhard B et al. Specialized coding of sensory, motor and cognitive variables in VTA dopamine neurons. Nature 570, 509–513 (2019). [PubMed: 31142844]
12. Yves K, Jérôme F, Clément R & Christian L Context-dependent multiplexing by individual VTA dopamine neurons. J. Neurosci 40, 7489–7509 (2020). [PubMed: 32859713]
13. Coddington LT & Dudman JT Review Learning from Action : Reconsidering Movement Signaling in Midbrain Dopamine Neuron Activity. Neuron 104, 63–77 (2019). [PubMed: 31600516]
14. Berke JD What does dopamine mean? Nat. Neurosci 21, 787–793 (2018). [PubMed: 29760524]
15. Watabe-Uchida M & Uchida N Multiple Dopamine Systems: Weal and Woe of Dopamine. Cold Spring Harb. Symp. Quant. Biol LXXXIII, 037648 (2019).
16. Aso Y et al. The neuronal architecture of the mushroom body provides a logic for associative learning. Elife 3, e04577 (2014). [PubMed: 25535793]
17. Claridge-Chang A et al. Writing Memories with Light-Addressable Reinforcement Circuitry. Cell 139, 405–415 (2009). [PubMed: 19837039]
18. Liu C et al. A subset of dopamine neurons signals reward for odour memory in Drosophila. Nature 488, 512–516 (2012). [PubMed: 22810589]
19. Aso Y et al. Specific dopaminergic neurons for the formation of labile aversive memory. Curr. Biol. 20, 1445–1451 (2010). [PubMed: 20637624]
20. Yamagata N et al. Distinct dopamine neurons mediate reward signals for short- and long-term memories. Proc. Natl. Acad. Sci. U. S. A 112, 578–83 (2015). [PubMed: 25548178]
21. Aso Y et al. Three Dopamine Pathways Induce Aversive Odor Memories with Different Stability. PLoS Genet. 8, e1002768 (2012). [PubMed: 22807684]
22. Aso Y & Rubin GM Dopaminergic neurons write and update memories with cell-type-specific rules. Elife 5, 1–15 (2016).
23. Aso Y et al. Mushroom body output neurons encode valence and guide memory-based action selection in Drosophila. Elife 3, e04580 (2014). [PubMed: 25535794]
24. Burke CJ et al. Layered reward signalling through octopamine and dopamine in Drosophila. Nature 492, 433–437 (2012). [PubMed: 23103875]
25. Hige T, Aso Y, Modi MN, Rubin GM & Turner GC Heterosynaptic Plasticity Underlies Aversive Olfactory Learning in Drosophila. Neuron 88, 985–998 (2015). [PubMed: 26637800]
26. Cohn R, Morantte I & Ruta V Coordinated and Compartmentalized Neuromodulation Shapes Sensory Processing in Drosophila. Cell 163, 1742–1755 (2015). [PubMed: 26687359]

27. Waddell S Neural Plasticity: Dopamine Tunes the Mushroom Body Output Network. Curr. Biol 26, R109–R112 (2016). [PubMed: 26859265]
28. Handler A et al. Distinct Dopamine Receptor Pathways Underlie the Temporal Sensitivity of Associative Learning. Cell 178, 60–75.e19 (2019). [PubMed: 31230716]
29. Berry JA, Cervantes-Sandoval I, Chakraborty M & Davis RL Sleep Facilitates Memory by Blocking Dopamine Neuron-Mediated Forgetting. Cell 161, 1656–1667 (2015). [PubMed: 26073942]
30. Aimon S et al. Fast near-whole–brain imaging in adult Drosophila during responses to stimuli and behavior. PLOS Biol. 17, e2006732 (2019). [PubMed: 30768592]
31. Siju KP et al. Valence and state-dependent population coding in dopaminergic neurons in the fly mushroom body. Curr. Biol 30, 809277 (2020).
32. Li F et al. The connectome of the adult Drosophila mushroom body provides insights into function. Elife 9, (2020).
33. Pnevmatikakis EA et al. Simultaneous Denoising, Deconvolution, and Demixing of Calcium Imaging Data. Neuron 89, 285–299 (2016). [PubMed: 26774160]
34. Patriarchi T et al. Ultrafast neuronal imaging of dopamine dynamics with designed genetically encoded sensors. Science (80-.). 360, (2018).
35. Dana H et al. Sensitive red protein calcium indicators for imaging neural activity. Elife 5, e12727 (2016). [PubMed: 27011354]
36. Hamid AA et al. Mesolimbic dopamine signals the value of work. Nat. Neurosci 19, 117–126 (2015). [PubMed: 26595651]
37. Coddington LT & Dudman JT The timing of action determines reward prediction signals in identified midbrain dopamine neurons. Nat. Neurosci 21, 1563–1573 (2018). [PubMed: 30323275]
38. Saunders BT, Richard JM, Margolis EB & Janak PH Dopamine neurons create Pavlovian conditioned stimuli with circuit-defined motivational properties. Nat. Neurosci 21, 1072–1083 (2018). [PubMed: 30038277]
39. Hughes RN et al. Ventral Tegmental Dopamine Neurons Control the Impulse Vector during Motivated Behavior. Curr. Biol 30, 2681–2694.e5 (2020). [PubMed: 32470362]
40. Syed ECJ et al. Action initiation shapes mesolimbic dopamine encoding of future rewards. Nat. Neurosci. 19, 34–36 (2016). [PubMed: 26642087]
41. Baker KL et al. Algorithms for Olfactory Search across Species. J. Neurosci 38, 9383–9389 (2018). [PubMed: 30381430]
42. Bell WJ & Kramer E Sex pheromone-stimulated orientation of the American cockroach on a servosphere apparatus. J. Chem. Ecol 6, 287–295 (1980).
43. Tsao CH, Chen CC, Lin CH, Yang HY & Lin S Drosophila mushroom bodies integrate hunger and satiety signals to control innate food-seeking behavior. Elife 7, 1–35 (2018).
44. Sayin S et al. A Neural Circuit Arbitrates between Persistence and Withdrawal in Hungry Drosophila. Neuron 544–558 (2019). doi:10.1016/j.neuron.2019.07.028 [PubMed: 31471123]
45. Yu Y et al. Regulation of starvation-induced hyperactivity by insulin and glucagon signaling in adult Drosophila. Elife 5, 1–19 (2016).
46. Landayan D, Feldman DS & Wolf FW Satiation state-dependent dopaminergic control of foraging in Drosophila. Sci. Rep 1–9 (2018). doi:10.1038/s41598-018-24217-1 [PubMed: 29311619]
47. Dayan P & Balleine BW Reward, Motivation, and Reinforcement Learning. Neuron 36, 285–298 (2002). [PubMed: 12383782]
48. Pang R, van Breugel F, Dickinson M, Riffell JA & Fairhall A History dependence in insect flight decisions during odor tracking. PLoS Comput. Biol 14, 1–26 (2018).
49. Jiang L & Litwin-Kumar A Models of heterogeneous dopamine signaling in an insect learning and memory center. PLOS Comput. Biol 17, e1009205 (2021). [PubMed: 34375329]
50. Takemura S et al. A connectome of a learning and memory center in the adult Drosophila brain. Elife 6, (2017).
51. Yamamoto K & Vernier P The evolution of dopamine systems in chordates. Front Neuroanat. 5, 1–21 (2011). [PubMed: 21373368]

52. Barron AB, Søvik E & Cornish JL The roles of dopamine and related compounds in reward-seeking behavior across animal phyla. Front. Behav. Neurosci 4, 163 (2010). [PubMed: 21048897]

53. Green J et al. A neural circuit architecture for angular integration in Drosophila. Nature 546, 101–106 (2017). [PubMed: 28538731]

54. Moore RJD et al. FicTrac: A visual method for tracking spherical motion and generating fictive animal paths. J. Neurosci. Methods 225, 106–119 (2014). [PubMed: 24491637]

55. Pnevmatikakis EA & Giovannucci A NoRMCorre: An online algorithm for piecewise rigid motion correction of calcium imaging data. J. Neurosci. Methods 291, 83–94 (2017). [PubMed: 28782629]

56. Giovannucci A et al. CaImAn an open source tool for scalable calcium imaging data analysis. Elife 8, (2019).

57. Meissner GW et al. An image resource of subdivided Drosophila GAL4-driver expression patterns for neuron-level searches. bioRxiv 2020.05.29.080473 (2020). doi:10.1101/2020.05.29.080473

58. Clements J et al. Analysis Tools for EM Connectomics. bioRxiv 2020.01.16.909465 (2020). doi:10.1101/2020.01.16.909465

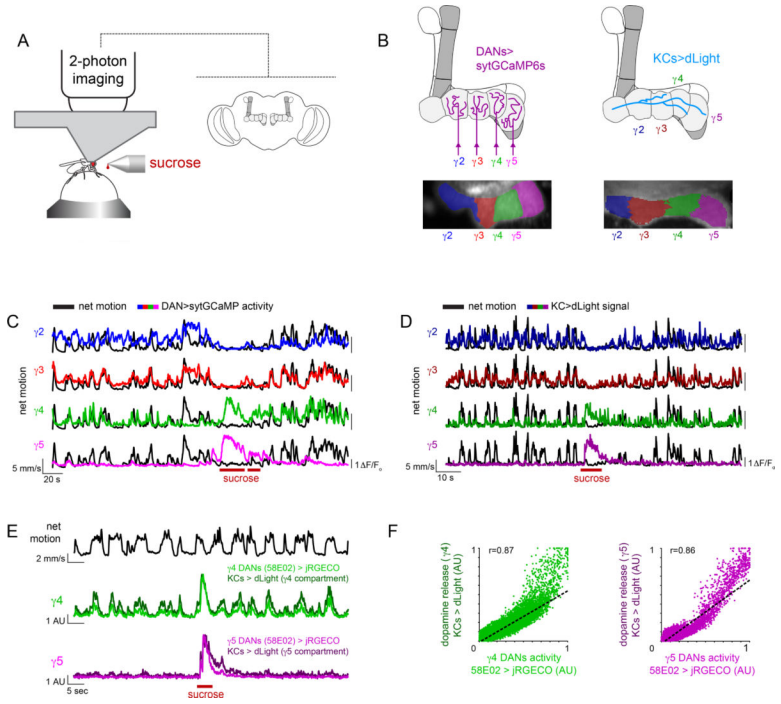

Figure 1. Compartmentalized DAN activity and dopamine release during reward and locomotion.

(A) Schematic of experimental system for recording mushroom body DAN activity during spontaneous locomotion and ingestion of sucrose reward (left). Cartoon of the mushroom body lobe anatomy within the *Drosophila* brain (right). **(B)** Schematic of compartmental organization of mushroom body lobes with DANs (top left) and Kenyon cell (KCs, top right) γ lobe innervation. Pixels in the γ lobe are color coded by K-means clustering analysis performed from recording sytGCaMP6s in DANs (bottom left) and dLight in KCs (bottom right) during periods of spontaneous locomotion demonstrating that correlated pixels align to the compartmentalized architecture of the lobe (γ2: blue, γ3: red, γ4: green, γ5: magenta). **(C)** Representative experiment overlaying the net motion (black) of a fly and DAN activity (colored) during spontaneous locomotion and ingestion of 1M sucrose (maroon bars). **(D)** Representative experiment overlaying the net motion (black) of a fly and KC dLight signaling (colored) during spontaneous locomotion and ingestion of 1M sucrose (maroon bars). **(E)** Overlay of DAN activity (γ4/5>jRGECO) and dopamine release (KC>dLight) during simultaneous recording aligned to net motion (top, black) during spontaneous locomotion and ingestion of 1M sucrose (maroon bars). **(F)** Relationships between γ4 (left) and γ5 (right) DAN and dLight activity. jRGECO and dLight signals normalized to trial minimum and maximum. Best fit line and Pearson correlation coefficient (r) indicated where relationship is statistically significant (p=10–20 with Bonferroni correction). N=5 animals, 17 trials.

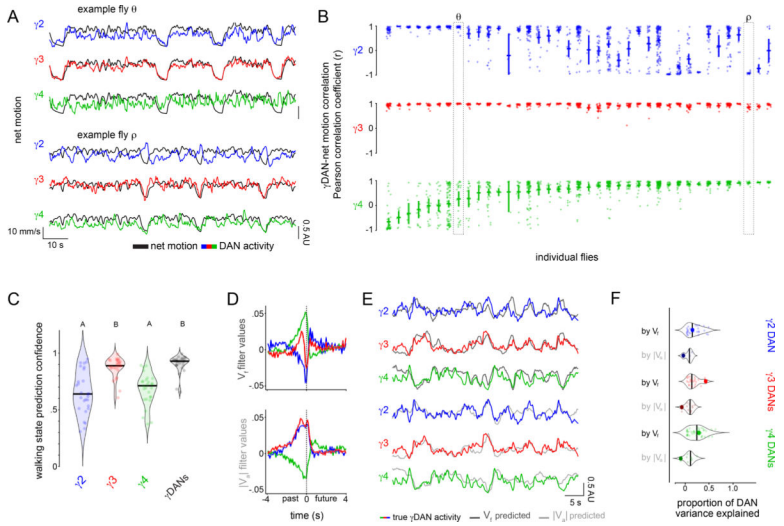

Figure 2. Differential encoding of behavior by mushroom body DANs.

(A) Representative experiments showing the variable relationship between the net motion (black) of a fly and DAN activity (colored) during bouts of spontaneous locomotion. Traces from flies θ and ρ are denoted in (B). **(B)** Pearson correlation coefficient between change in DAN activity and net motion at the onset of sustained locomotion (≥3 sec) following a pause (≥2 sec). Each column depicts all the bouts of movement initiation from an individual fly. Flies are ordered by the average correlation coefficient for γ4 DAN activity-net motion. N=39 animals, 1043 movement initiations. **(C)** Probability that a logistic regression model generated from DAN activity can accurately predict the locomotor state of an animal. N=27 animals. One-way ANOVA followed by Tukey's multiple comparison test. Data labeled with different letters are significantly different from each other ($p < 0.0001$). **(D)** Linear filters predicting DAN activity during bouts of continuous movement using forward velocity (V_f, top) or |angular velocity| ($|V_a|$), bottom) centered on an 8 second window. Plots include a 95% confidence interval that is obscured by the thickness of the average line. N=66 animals, recorded for 119 five-minute trials. **(E)** Overlay of true DAN activity (colored) and predicted DAN activity (gray) generated from linear filters in (D). **(F)** Proportion of variance ($R^2_{adjusted}$) of γ DAN activity explained by forward velocity and |angular velocity|. Example traces in (E) denoted by opaque point. N=66 animals, 119 five-minute trials.

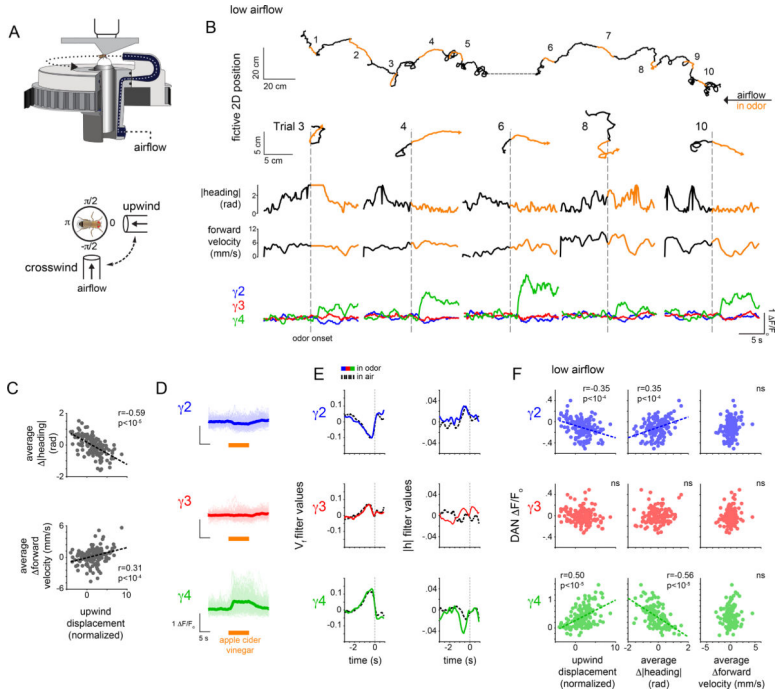

Figure 3. DAN activity during active odor tracking.

(A) Schematic of experimental paradigm (top) where a tethered fly's heading is yoked to a motor controlling the position of an air tube rotating around the fly. Bottom: top-down view of a tethered fly showing the position of the air tube during upwind and crosswind movement. **(B)** Top: Representative experiment depicting the fictive 2D trajectory in response to 10 presentations of apple cider vinegar (ACV). Animals were presented with clean air for 30 sec (black) and ACV for 10 sec (orange). Hash mark indicates a ~20 sec break in recording. Bottom: 2D trajectories (top row), |heading| (2nd row), forward velocity (third row), and γ DAN $\Delta F/F_o$ (bottom row) for trials in B. **(C)** Upwind displacement during the odor trial plotted vs Δ|heading| (top) and Δforward velocity (bottom) averaged throughout the odor presentation. Best fit line and Pearson coefficient (r) indicated where relationship is statistically significant (p<.001, Bonferroni correction, see Supplementary Table 2). Fisher r-to-z transformation indicates significant differences in correlation coefficients for upwind displacement - Δforward velocity and upwind displacement - Δ|heading| relationships with z=8.38. N=26 flies, 143 odor presentations. **(D)** γ DAN $\Delta F/F_o$ for all odor presentations, aligned to odor onset. Thick lines indicate average γ DAN activity. Translucent lines represent individual odor presentations. N=26 flies, 143 odor presentations. **(E)** Linear filters predicting DAN activity using forward velocity (V_f, left) or |heading| (|h|, right) in the odor plume (colored lines) and in clean air (black lines) over a 4 second window (zero mark indicates odor onset). N=26 flies, 143 odor presentations. **(F)** Average γ DAN $\Delta F/F_o$ vs normalized upwind displacement (left), average Δ|heading| (middle), and average Δforward velocity (right) during odor. Best fit line and Pearson coefficient (r) indicated where relationship is significant (p<.001, Bonferroni correction, see Supplementary Table 2). Fisher r-to-z transformation indicates significant differences in correlation coefficients for γ4-Δ|heading| and γ4-Δforward velocity relationship with z=−6.03. N=26 flies, 143 odor presentations.

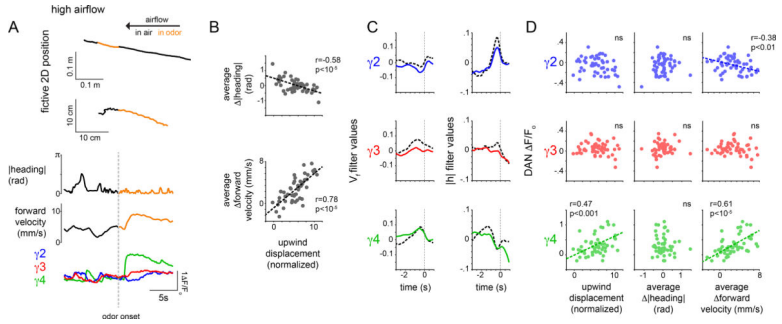

Figure 4. Mushroom body DAN activity - behavior correlations depend on a fly's navigational strategy.

(A) Representative experiment showing DAN activity and behavior under high airflow conditions. Top: fictive 2D trajectory during a 5 min trial with a 60 sec presentation of apple cider vinegar (orange). Second row: expanded view of the above trajectory, 20 sec period centered at odor onset. |heading| (third row) forward velocity (fourth row) and γ DAN activity (bottom) during that same 20 sec period. **(B)** Upwind displacement plotted as a function of average Δ|heading| (top) and average Δforward velocity (bottom) during odor presentation. Pearson coefficient (r) indicated where relationship is significant ($p<0.0001$, Bonferroni correction, see Supplementary Table 2). Fisher r-to-z transformation indicates significant differences in correlation coefficients with $z=-7.43$. Fisher r-to-z transformation also indicates significant differences in correlation coefficients for upwind displacement - Δforward velocity across the high and low airflow contexts with $z=-3.89$ but no significant differences in the correlation coefficients for upwind displacement - Δ|heading|. N=22 flies, 52 odor presentations. Linear filters predicting DAN activity using forward velocity (V_f, left) or |heading| (|h|), right) in the odor plume (colored) and in clean air (black, dashed) over a 4 second window (zero mark indicates odor onset). N=22 flies, 52 odor presentations. **(D)** Average γ DAN $\Delta F/F_o$ plotted as a function of net upwind displacement (left), average Δ|heading| (middle) and average Δforward velocity (right) during odor presentation. Pearson coefficient (r) indicated where relationship is significant ($p<.01$ with Bonferroni correction, see Supplementary Table 2). Fisher r-to-z transformation indicates significant differences in correlation coefficients for γ4-Δ|heading| and γ4-Δforward velocity relationship with $z=4.46$. Fisher r-to-z transformation indicates significant differences in correlation coefficients for γ4-Δ|heading| and γ4-Δforward velocity relationships across the high and low airflow contexts with $z=-1.77$ and $z=-3.42$, respectively. N=22 flies, 52 odor presentations.

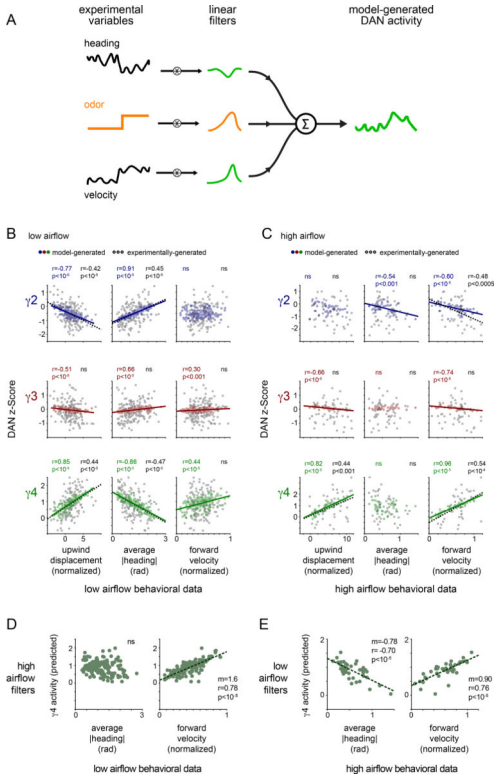

Figure 5. Analysis of dynamic DAN-motor correlations during odor pursuit.

(A) Schematic of analysis in which linear filters are applied to the experimental forward velocity or |heading| data to predict DAN activity over an odor trial (see methods for details). **(B)** Average predicted DAN activity plotted as a function of upwind displacement (left), |heading| (middle), and forward velocity (right) for each odor trial under low airflow conditions. Best fit line and Pearson correlation coefficient (r) indicated where relationship is statistically significant ($p<.01$ with Bonferroni correction, see Supplementary Table 2). N=26 flies, 143 odor presentations. **(C)** Average predicted DAN activity plotted as a function of experimentally determined upwind displacement (left), average |heading| (middle), and average forward velocity (right) for each odor trial under high airflow conditions. Best fit line and Pearson correlation coefficient (r) indicated where relationship is statistically significant ($p<.05$ with Bonferroni correction, see Supplementary Table 2). N=22 flies, 52 odor presentations. **(D)** γ4 DAN activity predicted by applying the high airflow filters to low airflow behavioral data, plotted as a function of experimentally-determined average |heading| (left) and average forward velocity (right) for each odor trial under low airflow conditions. Best fit line and Pearson correlation coefficient (r) indicated where relationship is statistically significant ($p<.01$ with Bonferroni correction, see Supplementary Table 2). N=26 flies, 143 odor presentations. **(E)** γ4 DAN activity predicted by applying the low airflow filters to high airflow behavioral data, plotted as a function of the experimentally-determined average |heading| (left) and average forward velocity (right) for each odor trial under high airflow conditions. Best fit line and Pearson correlation coefficient (r) indicated where relationship is statistically significant ($p<.01$ with Bonferroni correction, see Supplementary Table 2). N=22 flies, 52 odor presentations.

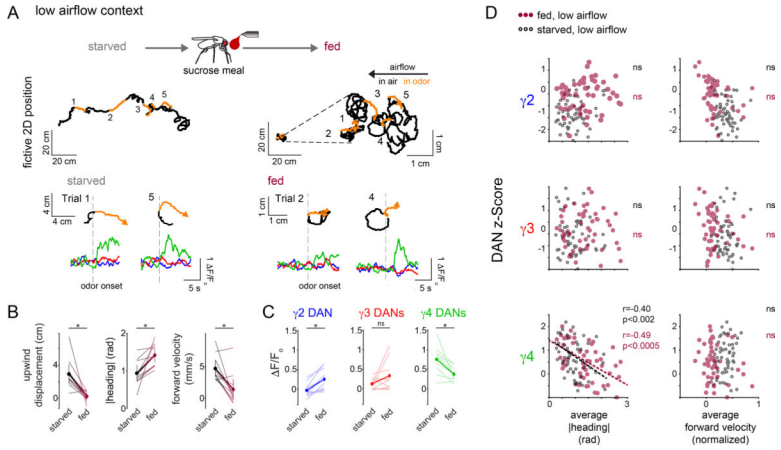

Figure 6. DAN responses and odor tracking behavior are altered by satiety state.

(A) Top: schematic depicting that DAN activity and behavior are measured in the same flies prior to (starved) and after consumption of a sucrose meal (fed). Middle: Representative experiment showing the 2D trajectory of a fly walking under low airflow conditions over a 5 min period in response to multiple presentations of apple cider vinegar (ACV, orange) prior to (starved, left) and after a sucrose meal (fed, right with inset zooming into behavior). Bottom: Comparison of indicated trajectories and γ DAN activity prior to and after feeding. **(B)** Behavioral responses to ACV are diminished once animals are fed. Upwind displacement (left), average |heading| (middle), and average forward velocity (left) of animals prior to (black, starved) and after (maroon, fed) a sucrose meal. Paired two-sided t-test with Bonferroni correction, $p<0.05$ (*), see Supplementary Table 2. N=10 flies, 102 odor presentations (49 before and 53 after feeding). **(C)** Average DAN responses to ACV are altered after feeding. Paired two-sided t-test with Bonferroni correction, $p<0.05$ (*), see Supplementary Table 2, N=10 flies, 102 odor presentations (49 before and 53 after sugar feeding). **(D)** The relationships between γ DAN activity and behavior in different satiety states. Average z score normalized DAN activity plotted as a function of average |heading| (left), and average forward velocity (right) during odor presentation prior to (black) and after (maroon) feeding. Fisher r-to-z transformation indicates no significant differences in correlation coefficients for γ4-|heading| relationship across starved and fed animals with $z=-0.51$. Pearson correlation coefficient (r) indicated where relationship is statistically significant ($p<0.02$ with Bonferroni correction, see Supplementary Table 2). N=10 flies, 49–53 odor presentations.

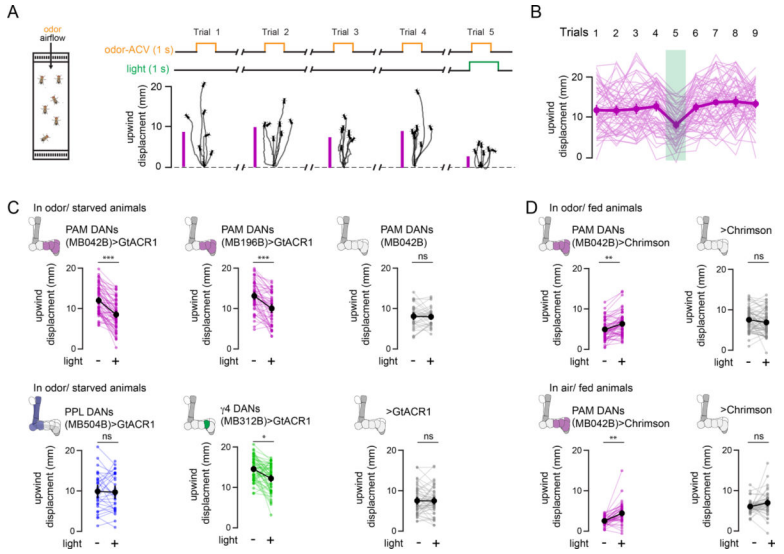

Figure 7. Optogenetic perturbations of DAN subsets acutely influences odor tracking.

(A) Left: Schematic of experimental chamber (left) in which 5–7 naïve flies in continuous laminar flow of clean air were presented with 10 1-sec trials of apple cider vinegar (ACV). On trial 5, the odor presentation was paired with optogenetic inhibition of indicated DAN subsets expressing GtACR1 or activation of DAN subsets expressing CsChrimson. Right: Representative experiment showing the trajectories of individual flies, aligned to common origin and wind direction. The average upwind displacement of all flies in the odor for each trial, measured as the change in center of mass along the axis of airflow is shown at left (magenta bars). **(B)** Upwind displacement of flies expressing GtACR in PAM DANs (MB042B driver). Thick dark line and circle marks indicate average behavior ± 95% confidence interval. Thin lines represent individual experiments. Trial where odor is paired with optogenetic inhibition is indicated by the green bar. N=63 experimental cohorts of 7 individual flies. **(C)** Average upwind displacement in the 4 odor presentations preceding optogenetic inhibition (−) and in the trial paired with optogenetic inhibition (+) for the indicated genotypes in starved animals. PAM DANs (MB042B driver)>GtACR1 (N=63, top left), PAM DANs (MB196B driver)>GtACR1 (N=49, top middle), PAM DANs MB042B-Gal4 parental controls (N=33, top right), PPL DANs (MB504B driver)>GtACR1 (N=30, bottom left), γ4 DANs (MB312B driver)>GtACR1 (N=54, bottom middle), UAS-GtACR1 parental controls (N=48, bottom right). Paired two-sided t-test with Bonferroni correction, $p<10^{-10}$ (***), $p<10^{-5}$ (**), $p<10^{-4}$ (*), see Supplementary Table 2. **(D)** Top: as in (C) but flies are fed and DANs are optogenetically activated with CsChrimson. N=60 paired cohorts of PAM DANs (MB042B driver)>CsChrimson and UAS-CsChrimson parental control animals assayed together during a single experiment. Bottom: average upwind displacement of fed animals in clean air without optogenetic activation (−) and with optogenetic activation (+) for the indicated genotypes. N=44 paired cohorts of PAM DANs (MB042B driver)>CsChrimson and UAS-CsChrimson parental controls animals assayed together during a single experiment. Paired t-test, two-sided, Bonferroni correction, $p<10^{-5}$ (**), see Supplementary Table 2.

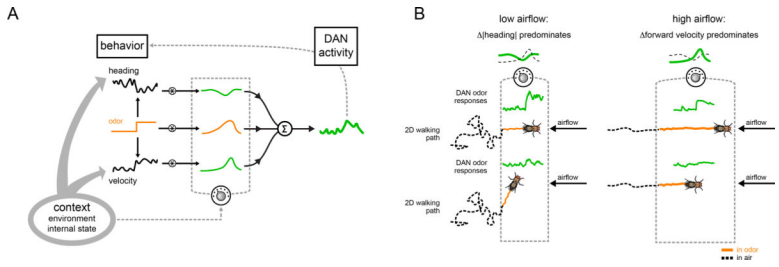

Figure 8. A model depicting how dynamic DAN-motor correlations emerge over different timescales.

(A) Schematic model showing how an animal's context, including whether it is walking spontaneously in clean air or engaged in active odor pursuit, the navigational strategy it employs, and its satiety state, shapes the moment-to-moment relationships between DAN activity and different behavioral variables (grey dial), giving rise to the longer timescale relationships in which DAN activity is preferentially tuned to the motor actions that subserve odor pursuit. An animal's context also coordinately influences behavior (thick grey arrows). Acute manipulation of DAN activity alters behavior, highlighting how the mushroom body dopaminergic system is embedded within a larger feedback loop (grey dashed arrow). **(B)** Schematic depicting how the model in (A) produces the behavior and neural activity we observe in the low (left) and high (right) airflow contexts. Under low airflow conditions (left), the γ4-|heading| relationship is selectively strengthened. When a fly encounters the odor, it reorients and elevated γ4 DAN activity promotes upwind tracking towards the odor source. Conversely, under high airflow conditions (right), the γ4 DAN activity-forward velocity relationship is selectively strengthened. When a fly encounters the odor, increased γ4 DAN activity also promotes upwind tracking towards the odor source despite a fly using different actions for pursuit.